NASA TECHNICAL NOTE

NASA TN D-7189

NASA TN D-7189

CHEMICAL NONEQUILIBRIUM EFFECTS ON THE INVISCID FLOW IN THE WINDWARD PLANE OF SYMMETRY OF TWO SIMPLIFIED SHUTTLE CONFIGURATIONS

by John A. Lordi, Robert J. Vidal, and Charles B. Johnson

Langley Research Center
Hampton, Va. 23365

NATIONAL AERONAUTICS AND SPACE ADMINISTRATION • WASHINGTON, D. C. • MARCH 1973

1. Report No.	2. Government Accession No.	3. Recipient's Catalog No.
NASA TN D-7189		

4. Title and Subtitle	5. Report Date
CHEMICAL NONEQUILIBRIUM EFFECTS ON THE INVISCID FLOW IN THE WINDWARD PLANE OF SYMMETRY OF TWO SIMPLIFIED SHUTTLE CONFIGURATIONS	March 1973
	6. Performing Organization Code

7. Author(s)	8. Performing Organization Report No.
John A. Lordi and Robert J. Vidal, Cornell Aeronautical Laboratory; and Charles B. Johnson	L-8477
	10. Work Unit No. 502-37-01-10
9. Performing Organization Name and Address	11. Contract or Grant No.
NASA Langley Research Center Hampton, Va. 23365	
	13. Type of Report and Period Covered
12. Sponsoring Agency Name and Address	Technical Note
National Aeronautics and Space Administration Washington, D.C. 20546	14. Sponsoring Agency Code

15. Supplementary Notes

Presented at Space Shuttle Aerothermodynamics Technology Conference, Ames Research Center, Moffett Field, California, December 1971.

16. Abstract

A theoretical study has been made to delineate some of the effects of thermochemical nonequilibrium in the inviscid flow field of a representative shuttle orbiter configuration. This study was based on experimental pressure data, obtained at the Langley Research Center, which was used as an input to the Cornell Aeronautical Laboratory reacting streamtube computer program. The pressure data from two configurations are tabulated. Calculations were restricted to the windward plane of symmetry, and the calculations covered an altitude range of from 60.96 to 76.20 km (200 000 to 250 000 ft) at velocities of 4.88 to 7.32 km/sec (16 000 to 24 000 ft/sec), respectively. Angles of attack of 20^{o} and 40^{o} were included as well as two nose radii, 0.305 and 1.22 meters (1 and 4 ft), and surface distances of approximately 40 nose radii.

The results of these calculations show that the nonequilibrium effects are confined largely to the entropy layer except at the highest altitude, where significant nonequilibrium effects are observed in the entire inviscid flow field. For the trajectory points considered, the oxygen remained fully dissociated for equilibrium and nonequilibrium flow in the entropy layer, and the principal nonequilibrium effects were caused by a lag in the nitrogen recombination reaction. The largest effect was observed in the translational temperature which can be lower or higher than the equilibrium value, depending on whether the streamline considered is processed by normal or oblique portions of the shock wave. The indications are that the boundary-layer development on the forward part of the body is governed by the nonequilibrium entropy layer. This results in boundary-layer transition which is earlier than predicted on the basis of equilibrium oblique shock wave conditions. The nonequilibrium effect on laminar heating rates in the nose region is a decrease of 30 to 40 percent if the wall is noncatalytic and if the boundary layer is frozen. The results obtained indicate that the viscous portion of the orbiter flow field can be far from equilibrium.

17. Key Words (Suggested by Author(s))	18. Distribution Statement
Nonequilibrium Inviscid flow Shuttle flight conditions	Unclassified – Unlimited

19. Security Classif. (of this report)	20. Security Classif. (of this page)	21. No. of Pages	22. Price*
Unclassified	Unclassified	45	$3.00

*For sale by the National Technical Information Service, Springfield, Virginia 22151

CHEMICAL NONEQUILIBRIUM EFFECTS ON THE INVISCID FLOW IN THE WINDWARD PLANE OF SYMMETRY OF TWO SIMPLIFIED SHUTTLE CONFIGURATIONS*

By John A. Lordi,** Robert J. Vidal,**
and Charles B. Johnson
Langley Research Center

SUMMARY

A theoretical study has been made to delineate some of the effects of thermochemical nonequilibrium in the inviscid flow field of a representative shuttle orbiter configuration. This study was based on experimental pressure data, obtained at the Langley Research Center, which were used as input to the Cornell Aeronautical Laboratory reacting stream-tube computer program. The pressure data from two configurations are tabulated. Calculations were restricted to the windward plane of symmetry, and the calculations covered an altitude range of 60.96 to 76.20 km (200 000 to 250 000 ft) at velocities of 4.88 to 7.32 km/sec (16 000 to 24 000 ft/sec), respectively. Angles of attack of 20° and 40° were included as well as two nose radii, 0.305 and 1.22 meters (1 and 4 ft), and surface distances of approximately 40 nose radii.

The results of these calculations show that the nonequilibrium effects are confined largely to the entropy layer except at the highest altitude, where significant nonequilibrium effects are observed in the entire inviscid flow field. For the trajectory points considered, the oxygen remained fully dissociated for equilibrium and nonequilibrium flow in the entropy layer, and the principal nonequilibrium effects were caused by a lag in the nitrogen recombination reaction. The largest effect was observed in the translational temperature which can be lower or higher than the equilibrium value, depending on whether the streamline considered is processed by normal or oblique portions of the shock wave. The indications are that the boundary-layer development on the forward part of the body is governed by the nonequilibrium entropy layer. This results in boundary-layer transition which is earlier than predicted on the basis of equilibrium oblique shock wave conditions. The nonequilibrium effect on laminar heating rates in the nose region is a decrease of 30 to 40 percent if the wall is noncatalytic and if the boundary layer is frozen. The results obtained indicate that the viscous portion of the orbiter flow field can be far from equilibrium.

---

*Presented at Space Shuttle Aerothermodynamics Technology Conference, Ames Research Center, Moffett Field, California, December 1971.

**Cornell Aeronautical Laboratory.

INTRODUCTION

The entry trajectory of the shuttle orbiter is designed for deceleration of the vehicle at high altitude. The resulting combination of low velocity at high altitude leads to significant departures from chemical equilibrium in the flow field for the portion of the flight where real-gas effects are important. Calculations have been made for the reacting flow along selected streamlines in the windward plane of symmetry of a blunted delta-wing shape representative of a shuttle orbiter.

An approximate model of the pressure field in the windward plane of symmetry of a blunted delta wing was constructed from wind-tunnel measurements of the body surface pressure distribution and approximate calculations of the shock shape and streamline locations. Numerical solutions for the flow along streamlines were then obtained for this pressure distribution. Solutions were obtained for both equilibrium and finite-reaction-rate nonequilibrium chemical reactions. Since the stream-tube solutions are much easier to compute than fully three-dimensional reacting flows, results could be obtained for a wide range of conditions. The validity of this approach is based on the assumptions that the pressure field is insensitive to nonequilibrium effects and that the flow along streamlines is quasi-one-dimensional. Numerical solutions have been used to verify this approach by making calculations on spherically blunted cones. (See ref. 1.)

The experimental surface pressure distributions were obtained in the Langley Mach 8 variable-density hypersonic tunnel (ref. 2). Pressure data were obtained for two representative shuttle test shapes, a blunted delta-wing body and a straight body, at angles of attack of 0°, 20°, 40°, and 60°. All these experimental results are presented, but the calculations for reacting flow were confined to angles of attack of 20° and 40°. The calculations for streamline flow were obtained with a computer program (ref. 3) previously developed at the Cornell Aeronautical Laboratory for the quasi-one-dimensional reacting flow of a general gas mixture. In the present work, air was assumed to be composed of N_2, O_2, NO, N, O, NO^+, e^-, and Ar. The thermodynamic and chemical kinetic data employed in the calculations are listed in reference 3.

The report first presents the data for the body surface pressure distributions. Next the approximate model of the pressure field in the windward plane of symmetry is described. Then results of both equilibrium and nonequilibrium flow calculations are discussed for three typical shuttle trajectory points in the altitude range of 60.96 to 76.20 km (200 000 to 250 000 ft) at velocities of 4.88 to 7.32 km/sec (16 000 to 24 000 ft/sec), respectively. Calculations are compared for two angles of attack, 20° and 40°, and two nose radii, 0.305 and 1.22 meters (1 and 4 ft). Finally, the implications of the departures from chemical equilibrium to shuttle technology are discussed. The questions of surface heating rates, boundary-layer transition, and entropy-layer swallowing are treated.

SYMBOLS

Values are given in both SI and U.S. Customary Units. The measurements and calculations were made in U.S. Customary Units.

b	span of model at row of spanwise pressure orifices
C	parameter defined in reference 4
C_f	local skin-friction coefficient
$F_c, F_{Rx}, F_{R\delta}$	transformation parameters defined in reference 5
H_T	total enthalpy
h	altitude, also static enthalpy
l	surface distance from Newtonian stagnation point to onset of transition
M	Mach number
n	velocity-profile power-law parameter
p	pressure
$\dot{q}$	heating rate
R	Reynolds number, $\rho_e V_e S / \mu_e$
R_N	nose radius
S	distance along streamline
T	temperature
u	velocity in boundary layer
V	velocity in inviscid flow field
x	distance along center line of body

y	normal distance from surface
z	surface distance measured perpendicular to model center line
α	angle of attack
β	parameter defined in equation (1)
γ	ratio of specific heats
δ	boundary-layer thickness
δ^*	displacement thickness
θ	momentum thickness
λ	sweep angle (complement of acute angle between free-stream flow direction and leading edge of swept surface)
μ	viscosity
ρ	density
τ	shear stress

Subscripts:

b	along surface from Newtonian stagnation point
eq	equilibrium
e	edge of boundary layer
f	frozen
L	body length, 23.5 cm (9.25 in.)
neq	nonequilibrium
t,1	total conditions in stagnation chamber

t,2	stagnation condition behind normal shock
w	wall conditions
∞	free-stream conditions
*	reference conditions

APPARATUS AND TEST PROCEDURES

A series of experiments were conducted in the Langley Mach 8 variable-density hypersonic tunnel to measure the windward surface pressure distributions on two simplified shuttle-type configurations. The models used were a blunted delta-wing model and a blunted straight-body model. (See fig. 1.) The tests were conducted at a nominal test-section Mach number of 8.0, unit Reynolds numbers in the range 8.8×10^6 to 41.5×10^6 per meter (2.68×10^6 to 12.65×10^6 per foot), and angles of attack of 0^o, 20^o, 40^o, and 60^o. The experimental test conditions are identified by run number and are listed in table I. The data obtained with the straight-body model are listed in table II and are given in the form $p/p_{t,2}$, where $p_{t,2}$ is the model stagnation pressure. The streamwise distance $\bar{s}/R_N$ is measured in the plane of symmetry starting from the Newtonian stagnation point at $\alpha = 0^o$. The spanwise distance z is measured from the model center line and is nondimensionalized by the local span b. The corresponding data obtained with the delta-wing body are given in table III.

EXPERIMENTAL TEST RESULTS

Schlieren photographs of the model flow field were obtained during each of the pressure tests. Typical results obtained with each of the two configurations are shown in figure 2 for angles of attack of 20^o, 40^o, and 60^o. A comparison of the schlieren photographs shown in figure 2 indicates that for $\alpha = 20^o$ (fig. 2(a)) the body shape has little effect on the shock shape. However, at $\alpha = 40^o$ (fig. 2(b)) the cross flow begins to affect the inviscid flow, and the result is a significant difference in the shock shape for the two bodies. At $\alpha = 60^o$ (fig. 2(c)) with greater cross flow the difference in shock shape is even more pronounced. The pressure data measured in the windward plane of symmetry are shown in figure 3 for both bodies at $\alpha = 20^o$, 40^o, and 60^o. The pressure data in figure 3 indicate quantitatively the same results that were indicated by the shock shapes in the schlieren photographs. At $\alpha = 20^o$ (fig. 3(a)) there is little difference in the pressure distributions for the two bodies; however, at $\alpha = 40^o$ (fig. 3(b)) there is a decay in the pressure level on the aft part of the straight body, whereas the delta-wing body has

almost a constant pressure downstream of $S/R_N \approx 5$. At $\alpha = 60^o$ (fig. 3(c)) both bodies show a decay in pressure due to cross-flow effects, but the straight body has a more significant pressure decrease due to the larger cross flow. The solid line in figures 3(a) and (b) is the fairing of the pressure data that were used as input to the nonequilibrium calculations.

FLOW-FIELD CALCULATIONS

In a previous study (ref. 1) of the hypersonic flow over blunted slender cones, the surface pressure distribution was found to be insensitive to nonequilibrium effects. The flow along the windward plane of symmetry of the blunted delta wing should be similar to the flow over a blunt cone; this fact has been used in the present study to scale the measured pressure distributions to flight conditions. The data were normalized by the stagnation pressure on the tunnel model, and the pressures on the full-scale vehicle were obtained by using the appropriate value of the stagnation pressure. The initial portion of the pressure distribution, that is, between the stagnation point and the first data point, was taken from a composite correlation (ref. 1) of ideal gas, equilibrium and nonequilibrium flow calculations, and experimental data for the flow over spherically blunted bodies. The stagnation point was assumed to be the point where the body surface is normal to the free-stream direction. A full-scale body length of 45.7 meters (150 ft) was used.

The body surface pressure distributions which were used in the stream-tube calculations for $\alpha = 20^o$ and $\alpha = 40^o$ are shown in figures 3(a) and (b), together with the experimental data on which they are based. The distance along the surface streamline S_b is measured from the stagnation point.

The pressure histories along streamlines off the body surface were obtained by using an approximate model of the pressure field. The shock shapes and streamline locations were obtained for equilibrium flow, and again the results for the flow about blunted cones were used (ref. 1). These results indicate that the shock shape as well as the surface pressure is insensitive to nonequilibrium effects.

The bow shock wave was assumed to be circular in the nose region and straight on the afterbody. The circular portion of the shock was not taken to be concentric with the body. Rather, the center and radius of curvature were found by using a correlation for shock standoff distance at the stagnation point (ref. 6) and a mass balance to determine the shock standoff distance at the body shoulder. The mass balance was obtained by assuming the flow in the stagnation region of the windward plane of symmetry to be the same as that in the axisymmetric flow over a blunted cone. The circular portion of the shock was joined to the straight portion at the point of tangency. The final shock angle for the straight portion was determined from the asymptotic, experimental surface pressure and oblique shock solutions for equilibrium flow. In the nose region, the streamline

locations also were found by using a mass-balance technique. The mass flux was assumed to vary linearly from the shock to the body along normals to the body surface. The solution for the equilibrium flow along the body streamline was computed by using the known pressure distribution and an isentropic expansion from the known stagnation conditions. The values at the shock were obtained from the shock angle and shock tables for equilibrium flow (ref. 7). In the afterbody region the streamlines were assumed to be parallel to the body. This assumption of a uniform pressure field on the afterbody appears justified both by schlieren photographs obtained in this study (fig. 2) and by three-dimensional flow calculations for equilibrium flow over a blunted delta wing (ref. 8). After the streamline locations had been established, the pressure distributions along them were computed by assuming a linear variation along normals to the body between the pressure at the body and the shock.

The shock shape and streamline pattern obtained for $\alpha = 20^{\circ}$ and $\alpha = 40^{\circ}$ are shown in figure 4. The flow field consists basically of two regions: those streamlines which are processed by the strong curved shock and those which pass through the limiting oblique shock. The streamline which passes through the point where the shock becomes straight is referred to as the outer streamline or oblique-shock streamline. The pressure field between this streamline and the shock is assumed to be uniform. While these streamline locations may not be precise, the important point is that the pressure histories are realistic and the streamline calculations provide an accurate assessment of the nonequilibrium flow effects. Furthermore, for the extreme cases of the body surface streamline and the outer streamline, the calculations are good approximations to the results obtained from more general flow-field calculations.

RESULTS AND DISCUSSION OF THEORETICAL CALCULATIONS

Calculations of the flow along selected streamlines, in the windward plane of symmetry using the experimental pressure distribution previously described, have been made for both equilibrium and nonequilibrium chemical reactions. The trajectory points at which streamline calculations were made are as follows:

1. V_{∞} = 4.877 km/sec (16 000 ft/sec); h = 60.96 km (200 000 ft)
2. V_{∞} = 6.096 km/sec (20 000 ft/sec); h = 67.06 km (220 000 ft)
3. V_{∞} = 7.315 km/sec (24 000 ft/sec); h = 76.20 km (250 000 ft)

The calculations were made for points along the body surface streamline, a streamline about in the middle of the entropy layer, and the outer streamline, which passes through the limiting oblique shock. The influence of changes in angle of attack and nose radius was also examined.

Although the presence of ionization was allowed for in the calculations, the results for the electron concentration have not been presented in detail. However, the effect of nonequilibrium on the ionization and deionization reactions is even more pronounced than on the neutral chemistry. For the range of conditions considered herein, the electron number densities were between 10^{13} and 10^{14} cm^{-3} in the nose region and between 10^{11} and 10^{12} cm^{-3} at the base of the body.

The basic nonequilibrium processes are different for those streamlines near the body and for the outer streamlines. In the entropy layer, that is, along the streamlines near the body surface, the flow approaches chemical equilibrium in the stagnation region and then departs from equilibrium in the rapid expansion of the flow around the nose of the body. Along the outer streamlines, the flow is very much like the relaxing flow behind a shock wave. That is, the flow is chemically frozen through the shock wave and then relaxes toward equilibrium over the entire body length. Thus, near the body surface the departure from equilibrium is a lag in the rate of recombination as the flow expands from the stagnation point, while along the outer streamlines there is a lag in the dissociation rate.

Body Streamline

Several calculations have been made for the flow along the body surface streamline, starting from an equilibrium stagnation point. In the altitude range of 60.96 to 76.20 km (200 000 to 250 000 ft), the flow along the body surface streamline is composed mainly of N_2, N, and O for both equilibrium and nonequilibrium flow. In both cases the oxygen is fully dissociated and remains so. The principal nonequilibrium effect is the lag in the nitrogen atom recombination as the flow expands in the nose region. The variation in species concentrations along the streamline is shown in figure 5, and the variation of temperature, density, and velocity along the streamline is illustrated in figures 6(a) to (c) for the trajectory point V_∞ = 4.877 km/sec (16 000 ft/sec), h = 60.96 km (200 000 ft), for R_N = 1.22 meters (4 ft), and $\alpha = 20^o$.

The temperature distribution (fig. 6(a)) is a direct consequence of the nonequilibrium effect on the nitrogen atom recombination rate. The nonequilibrium flow temperature falls much below the equilibrium temperature in the nose region because the nitrogen atom recombination reaction becomes frozen. Then, in the fairly uniform flow on the flat aft surface, some recombination takes place and the nonequilibrium temperature relaxes toward the equilibrium value near the base of the body. It should be noted that this approach is gradual and the flow is almost frozen over the entire body. The nonequilibrium effects on density (fig. 6(b)) and velocity (fig. 6(c)) are in directions such that there is very little effect on the mass flow rate.

Numerical solutions were obtained for the equilibrium and nonequilibrium flow along the body streamline for the three trajectory points given previously. These calculations were performed for an angle of attack of 20^{o} and a body nose radius of 1.22 meters (4 ft). The change in the nonequilibrium effects from one trajectory point to the next is one of degree rather than kind. In this series of calculations, the temperature distributions are all similar to that shown in figure 6(a), and therefore the difference between the equilibrium and nonequilibrium flow temperatures at the base of the body is a good measure of the effect of nonequilibrium chemical reaction on the body streamline flow for these conditions. The temperatures at the base of the body are listed in table IV for the three trajectory points at which calculations were made. The difference between the equilibrium and nonequilibrium temperatures is greatest at the highest altitude and highest velocity point and amounts to about 35 percent of the equilibrium value. This stems from the fact that nitrogen dissociation is greatest at this trajectory point and the most energy is frozen in chemical composition for this case.

Outer Streamline

The flow along the outer streamline in the flow field of the blunted delta wing is much like the flow behind an oblique shock wave. The reacting flow behind strong shock waves was extensively reviewed in reference 9, in which several calculations were made to investigate scaling and distances to equilibrium. In addition, it was shown in reference 9 that the mapping of normal shock wave flows to approximate wedge flows was quite accurate, and a similar technique was used in the calculations made for this report.

The results found here are very much in line with what would be expected in terms of the flow behind such equivalent normal shocks. At the velocities and altitudes of interest, the distances to equilibrium can be considerable. For an angle of attack of 20^{o}, the shock angle determined by the limiting pressure ratio is about 25^{o}, and it varies little from one trajectory point to the next. The flow behind this wave, computed here as a constant-pressure streamline flow, is essentially frozen over the length of the vehicle. The temperature at a distance of 45.7 meters (150 ft) from the shock wave is shown for three trajectory points in table V. At the lowest altitude of interest, it can be seen that the flow is essentially an ideal gas flow. At the highest velocity and highest altitude, the difference between the equilibrium and nonequilibrium flow temperature is appreciable, about 38 percent of the equilibrium value. Along the outer streamline this discrepancy is due mainly to a lag in the oxygen dissociation rate and nitric oxide formation while the nitrogen remains virtually undissociated.

The manner in which chemical nonequilibrium effects change, as attention is focused in turn on streamlines near the body surface and then on streamlines farther out in the shock layer, was briefly described previously. Along the body streamline, the static temperature of the nonequilibrium flow falls significantly below the equilibrium flow value as

the flow expands around the nose. Along the outer streamlines, the temperature in the nonequilibrium flow decreases toward the equilibrium value as the flow approaches chemical equilibrium. The flow along several streamlines in the shock layer has been computed for one of the trajectory points $\left(V_\infty = 4.877 \text{ km/sec (16 000 ft/sec)}, \ h = 60.96 \text{ km (200 000 ft)}, \ \alpha = 20^\circ\right)$. The results for the variation of the temperature normal to the body surface are shown in figure 7 for $S_b/R_N = 30$. The relative values for equilibrium and nonequilibrium flow reflect the behavior of the flow chemistry, as described previously. For this case the flow along the streamlines outside the entropy layer is essentially an ideal gas flow.

Effect of Angle of Attack

Streamline calculations have also been made at $\alpha = 40^\circ$, and these, combined with previous calculations, provide an indication of the influence of angle of attack on chemical nonequilibrium based on the delta-body distribution only. At this angle of attack the flow expansion around the nose of the body is weaker. Hence there is less of a lag in the recombination rate for nitrogen atoms. The density level is higher (on the afterbody), and the flow approaches equilibrium much more rapidly than for $\alpha = 20^\circ$, both along the body streamlines and along the outer streamlines. The temperature distributions along the body streamline and along the outermost streamline are illustrated in figures 8 and 9 for $V_\infty = 4.877$ km/sec (16 000 ft/sec), $h = 60.96$ km (200 000 ft), and $R_N = 1.22$ meters (4 ft). Again, these are typical of the results at other trajectory points considered in this study.

Effect of Nose Radius

The flow along the outer streamline is, of course, dependent only on the distance from the bow wave and is not influenced by the body nose radius. On the other hand, the flow along the streamlines in the entropy layer is affected by changes in body scale or nose bluntness. In the present framework, a change in body nose radius changes the rate at which the pressure drops in the expansion around the blunt nose. The rate of this pressure drop determines the departure from equilibrium. In order to investigate the effect of nose radius, the body streamline calculations for $\alpha = 20^\circ$ were repeated for a body nose radius of 0.305 meter (1 ft). Again, the temperature variation along the streamline has been used to characterize the nonequilibrium effects. The equilibrium solution and the nonequilibrium solutions for $R_N = 0.305$ and 1.22 meters (1 and 4 ft) are compared in figure 10. These results show that very little more energy is frozen in the expansion around the smaller nose, which means that little additional freezing occurs when the shoulder expansion is accomplished in one-fourth the distance. Furthermore, at large distances from the nose it is expected that temperatures for both nose radii should agree closely. These results are typical for the range of trajectory points considered

and for nose radii in the 0.305- to 1.22-meter (1- to 4-ft) range. The flow along the body streamline becomes frozen in the expansion around the blunt nose and recombines only a slight amount over the body lengths of interest.

Inviscid Nonequilibrium Effects on Heating Rates

Estimates of surface heating rates depend on the inviscid-flow calculation through the various edge conditions used in the boundary-layer calculations. For example, consider the laminar-heat-transfer rate in the nose region. For a chemically frozen boundary layer on a noncatalytic surface, a local similarity calculation shows that the heat-transfer rate is proportional to $\sqrt{\rho_w u_e}\left(H_{T,f} - h_w\right)$, where $H_{T,f}$ is the total frozen enthalpy, ρ_w is the density at the wall, and u_e is the velocity at the edge of the boundary layer. The laminar heating rates for equilibrium and nonequilibrium inviscid flow have been estimated by using this result and assuming that the body streamline typifies the edge conditions. The results, the ratio of nonequilibrium to equilibrium heating rates, are shown in figure 11. These are shown for $V_\infty = 7.315$ km/sec (24 000 ft/sec), $h = 76.20$ km (250 000 ft), $\alpha = 20^\circ$, $R_N = 1.22$ meters (4 ft).

The assumption of frozen boundary-layer flow was chosen as a point of comparison because the inviscid flow becomes frozen in the corner expansion and this indicates that the chemical state of the boundary layer will be far from equilibrium. It should also be noted that if the surface is completely catalytic the surface heat-transfer rate depends very little on the chemical state of the boundary layer. Furthermore, the only way that nonequilibrium effects would then be important is through the transport properties.

In order to calculate accurately the influence of the inviscid flow on the surface heating rate, the "swallowing" of the inviscid flow by the boundary layer should be accounted for. Although this was not done in the above calculation, it is noted that calculations of the boundary-layer thickness indicate that the boundary layer is thin compared with the shock layer. Thus, in the nose region the streamlines in the entropy layer, where nonequilibrium effects are most severe, determine the boundary-layer edge conditions.

The entropy layer will be swallowed at some point along the body and the boundary-layer edge conditions near the base of the body are determined by the outer streamline of the inviscid flow. The ratio of $H_{T,f} - h_w$ for nonequilibrium flow to that for equilibrium flow along the outer streamline is about 1.07 for the highest altitude and highest velocity case considered herein. Although the static temperatures are considerably different for the equilibrium and nonequilibrium flow along this streamline, the frozen total enthalpy is not appreciably affected because the flow is a high Mach number flow and the static enthalpy is small compared with the total. Hence the nonequilibrium effects on the flow in

the outer streamline do not appear to have much of an effect on the surface heat-transfer rate at low angles of attack.

Transition and Entropy-Layer Swallowing

The results of the inviscid stream-tube computations have been applied to estimate boundary-layer transition, the thicknesses of the laminar and turbulent boundary layers, and the location in the flow field where the entropy layer will be fully consumed by the boundary layer, that is, entropy-layer swallowing. Transition estimates were based on the transition criterion described in reference 10 and used in reference 11. For $\alpha = 20^{\circ}$, this criterion requires $\dfrac{R_{e,\theta}}{M_e\left(\dfrac{R_e}{ft}\right)^{1/5}} \approx 10$. The same interim criterion recommends that the Reynolds number based on momentum thickness be estimated with the following formulas,

$$R_{e,\theta} = 0.664\sqrt{\frac{\rho_*\mu_*}{\rho_e\mu_e}}\sqrt{\frac{R_{e,l}}{\beta}} \tag{1}$$

where

$$\frac{T_*}{T_e} = \frac{1}{2}\left(\frac{T_w}{T_e} + 1 + 0.07471M_e^2\right)$$

and

$$\beta = 1.0 + 0.745\sqrt{\frac{\gamma - 1}{2}}\tan\alpha\tan\lambda$$

where α and λ are the angle of attack and the sweep angle, respectively. These formulas have been used to cast the transition criterion into a form to yield the transition length as

$$l = 226.8\beta\frac{\rho_e\mu_e}{\rho_*\mu_*}\frac{M_e^2}{\left(R_e/ft\right)^{3/5}} \tag{2}$$

This form of the transition criterion shows that the transition length varies as the square of the Mach number or inversely as the temperature.

The laminar boundary-layer thicknesses were estimated from Cheng's two-dimensional local similarity solution (ref. 4), generalized to relax the hypersonic approximations and to obtain a solution based on boundary-layer edge conditions. Omitting the details of this development, the relation that is obtained for the displacement thickness is

$$\frac{\delta^*}{S_b} = 0.664 \frac{\gamma - 1}{2} M_e^2 \sqrt{\frac{C}{R_{e,S_b}}} + 1.73 \frac{T_w}{T_{t,1}} \left(1 + \frac{\gamma - 1}{2} M_e^2\right) \sqrt{\frac{C}{R_{e,S_b}}} \tag{3}$$

where in this case $C = \frac{\mu_w}{\mu_e} \frac{T_e}{T_w}$. The net effect of relaxing the hypersonic restriction is to retain the term 1 in the last parameter $1 + \frac{\gamma - 1}{2} M_e^2$. The displacement thickness was taken to be the boundary-layer thickness, which is a good approximation for high-speed flows.

For the present purposes, it was assumed that the boundary layer was fully turbulent immediately following transition, and the thickness estimates were based on the Spalding-Chi theory (ref. 5) and on procedures given by Johnson (ref. 12). The Spalding-Chi theory was approximated by a logarithmic law $F_c C_f \approx 0.039 \left(F_{Rx} R_{e,x}\right)^{-1/6}$ with errors of less than 10 percent, and this was applied in the usual momentum integral relation for boundary-layer thickness. That is

$$\tau(x) = \rho_e u_e^2 \frac{d\theta}{dS_b} = \rho_e u_e^2 \frac{n}{(n + 1)(n + 2)} \frac{d\delta}{dS_b} \tag{4}$$

and solving for the boundary-layer thickness gives

$$\delta = \frac{(n + 1)(n + 2)}{2n} \int_0^{S_b} C_f \, dx \tag{5}$$

where n is defined from $\frac{u}{u_e} = \left(\frac{y}{\delta}\right)^{1/n}$. This expression, combined with the above approximation to the Spalding-Chi theory, yields

$$\frac{\delta}{S_b} = 0.0468 \frac{(n + 1)(n + 2)}{2n} \frac{1}{F_c} \left(\frac{F_c}{F_{R\delta} R_{e,S_b}}\right)^{1/6} \tag{6}$$

The exponent in the power-law velocity profile was determined from a correlation found in reference 12. The distance to the virtual origin of turbulent flow which is required in the correlating parameter was determined from the correlation for an assumed Blasius profile (n = 1.04) and using the local flow properties at the start of transition.

The location of transition and the boundary-layer thickness were determined by using the various nonequilibrium streamlines in the entropy layer for edge conditions and by using an equilibrium streamline processed by the oblique shock wave. The latter is often used in calculating boundary-layer characteristics, and the results of the calculations provide some indication of the validity of using this procedure.

The results of the boundary-layer and transition calculations are shown in figure 12 for the three trajectory points considered herein and for an angle of attack of 20°. For an altitude of 60.96 km (200 000 ft) (fig. 12(a)), the calculations show that the laminar boundary-layer thickness is insensitive to the edge conditions, but transition is strongly influenced. The streamlines are labeled according to their distance from the body surface. The transition location varies by a factor of $2\frac{1}{2}$, depending on whether the nonequilibrium body streamline or the oblique-shock streamline is used. For these flight conditions, the latter corresponds to an ideal-gas streamline, and there are essentially no nonequilibrium effects in that portion of the flow field.

Indicated in figure 12 is an approximate edge of the entropy layer, which corresponds to the shock standoff distance at the shoulder of the spherical nose. The limitations in this approximation are recognized in that it neglects displacement effects on the entropy layer, nonequilibrium effects on the shock standoff distance, and so forth. However, this approximate edge of the entropy layer probably is conservative in that the effects cited would displace it farther from the body. However, it does yield a meaningful estimate of entropy-layer swallowing. It can be seen in figure 12(a) that the laminar boundary layer and transition are governed by conditions in the nonequilibrium entropy layer. The dominant nonequilibrium effect in this region is in the static temperature, and it differs from the equilibrium value by about 30 percent. This enters into the criterion for transition length through the square of the Mach number. Along the body streamline the nonequilibrium effect on temperature results in an increase in transition length.

It can be seen in figure 12(a) that after transition, the boundary layer thickens rapidly, and it is thicker by about a factor of 2 where the nonequilibrium entropy layer governs the flow. These boundary-layer estimates indicate that the nonequilibrium entropy layer is fully swallowed in the boundary layer at a distance of about $S_b/R_N \approx 20$ if the equilibrium outer streamline (oblique shock) edge conditions are used. For the other edge conditions the boundary layer on the nonequilibrium streamlines has a considerably shorter entropy swallowing distance. This means that the boundary-layer develop-

ment on the forward part of the body is governed by the nonequilibrium entropy layer, and the boundary layer on the aft part can be estimated using conditions based on the oblique shock wave.

The calculated boundary-layer characteristics at an altitude of 67.06 km (220 000 ft) are shown in figure 12(b). These show that the thickness of the laminar layer is influenced by the edge conditions and that the laminar layer develops under conditions corresponding approximately to the nonequilibrium body streamline. These results show that the transition length is a factor of 4 shorter than predicted by use of equilibrium oblique-shock conditions. The approximate thickness of the nonequilibrium entropy layer is shown in figure 12(b), and it can be seen that much of the boundary layer develops under the influence of the nonequilibrium entropy layer. For this flight condition the nonequilibrium entropy layer is fully swallowed by the boundary layer at about $S_b/R_N = 16$. Again, the forward part of the boundary layer is governed by nonequilibrium conditions in the entropy layer while the aft part is governed by the conditions behind the oblique shock wave.

The calculated boundary-layer characteristics at an altitude of 76.20 km (250 000 ft) are shown in figure 12(c). These show that the thickness of the laminar boundary layer is influenced appreciably by the assumed edge conditions, differing in thickness by a factor of 2 for the two nonequilibrium streamlines considered, with the thinner boundary layer calculated for the edge conditions of the nonequilibrium body streamline. Again, transition is strongly and adversely affected by the nonequilibrium entropy layer and is predicted to occur at $S_b/R_N = 5$ as compared with the prediction based on the equilibrium oblique shock conditions at $S_b/R_N = 17$. For this flight condition, the entire inviscid flow field is affected by thermochemical nonequilibrium, and it is not appropriate to calculate streamline conditions based on equilibrium flow behind the oblique shock. The streamline at $y/R_N = 0.1$ is processed by the oblique wave, and the nonequilibrium effects on boundary-layer thickness can be seen by comparing the results for that streamline with those for the equilibrium oblique-shock streamline. The entropy layer is thinner than at the lower altitudes, and the indications are that for the nonequilibrium outer streamline it will be swallowed by the boundary layer at about 13 nose radii from the leading edge. For this case, the entire inviscid flow field is influenced by nonequilibrium effects.

CONCLUDING REMARKS

The degree of chemical nonequilibrium in the inviscid flow field of a blunted delta-wing body, typical of a shuttle-type configuration, was examined within the framework of numerical calculations of the reacting flow along selected streamlines in the windward plane of symmetry. An approximate model of the pressure field was devised, on the

basis of experimental data, and the reacting streamline flows were computed for specified pressure histories.

Pressure data obtained in the Langley Mach 8 variable-density hypersonic tunnel on two test shapes, a blunted delta-wing body and a straight body were presented for angles of attack of 0°, 20°, 40°, and 60°. Streamline calculations were performed for three typical trajectory points in the altitude range of 60.96 to 76.20 km (200 000 to 250 000 ft) at velocities of 4.88 to 7.32 km/sec (16 000 to 24 000 ft/sec), respectively. Results were obtained for two angles of attack, 20° and 40°, and for two nose radii, 0.305 and 1.22 meters (1 and 4 ft), and surface distances of approximately 40 nose radii.

Most of the calculations were made for the 20° angle of attack and the 1.22-meter (4-ft) nose radius. The results for these cases were very similar over the range of trajectory points considered. On the streamlines close to the body, the flow approaches chemical equilibrium in the stagnation region and then freezes in the expansion around the spherical nose. Along the inner streamlines the flow is composed of essentially N_2, N, and O for the conditions treated. Along the outer streamlines, the flow was essentially frozen for the 20° angle of attack. The difference between the equilibrium and nonequilibrium solutions became appreciable at the highest trajectory point considered.

The effect of angle of attack was investigated by computing streamline flows for 40° and comparing them with the 20° results. The increase in density level on the windward surface was sufficient to promote an approach to chemical equilibrium along both the inner and outer streamlines in the shock layer. The calculations carried out indicated very little effect of nose radius on the degree of nonequilibrium since the flow along the body streamline freezes even for larger values of the nose radius. The streamlines outside the entropy layer are independent of nose bluntness effects.

The edge conditions of the laminar boundary layer in the nose region are determined by streamlines which pass through the nearly normal portion of the bow shock. On the other hand, the streamlines which pass through the limiting oblique shock determine the edge conditions of the boundary layer toward the base of the body. The calculations made here for an angle of attack of 20° show that a fairly large fraction of the total enthalpy, for example, about 30 percent, can be frozen in the chemistry along the body streamlines. On the other hand, in the flow along the outer streamlines the chemistry is nearly frozen but this accounts for less than 10 percent of the total enthalpy. As the angle of attack increases, the fraction of the total enthalpy attributed to dissociation increases, but so does the rate of dissociation. At an angle of attack of 40°, the flow in the outer streamlines is near equilibrium over most of the length of the vehicle.

The influence of nonequilibrium effects on the boundary layer has been estimated by means of approximate boundary-layer calculations. These results show that for all three trajectory points, the laminar boundary-layer development is governed by the nonequilib-

rium entropy layer. In each case, transition is determined by conditions in the nonequilibrium entropy layer and not by conditions behind the oblique wave. The boundary-layer development on the aft portions is governed by equilibrium flow behind the shock at the two lower altitudes and by nonequilibrium flow behind the oblique shock wave at the highest altitude.

There are several features of the nonequilibrium flow over a shuttle orbiter which should be mentioned. First, it should be noted that the flow in the windward plane of symmetry does not necessarily represent the upper limit as far as chemical nonequilibrium effects are concerned. One part of the flow that is subject to a much greater expansion than in the plane of symmetry is that part along streamlines which enter the nearly normal portion of the bow shock on the windward side but are then swept around the edge of the body to the leeward side. Consequently, the difference between the equilibrium and nonequilibrium flow properties and composition along such streamlines could be greater than along those treated in this study.

The results of the present study indicate that nonequilibrium effects will persist at altitudes below 60.96 km (200 000 ft) for those streamlines near the body surface. Also, nonequilibrium effects along the outer streamlines could be important at higher angles of attack at altitudes above 76.20 km (250 000 ft).

For the range of trajectory points considered herein, nonequilibrium effects are most important in the entropy layer. However, there are significant effects on temperature and composition throughout the flow field in some portions of the orbiter entry trajectory. The influence of the nonequilibrium effects on the boundary-layer edge conditions has been shown to be significant. Furthermore, the results of the present work indicate that the flow in the boundary layer can be far from equilibrium in the altitude range above 60.96 km (200 000 ft).

Langley Research Center,
National Aeronautics and Space Administration,
Hampton, Va., January 31, 1973.

REFERENCES

1. Wittliff, C. E.; and Sundaram, T. R.: A Study of Real-Gas Effects on Blunted Cone Flows. AEDC-TR-69-36, U.S. Air Force, Jan. 1969. (Available from DDC as AD 847 062.)

2. Schaefer, William T., Jr.: Characteristics of Major Active Wind Tunnels at the Langley Research Center. NASA TM X-1130, 1965.

3. Lordi, J. A.; Mates, R. E.; and Moselle, J. R.: Computer Program for the Numerical Solution of Nonequilibrium Expansions of Reacting Gas Mixtures. NASA CR-472, 1966.

4. Cheng, H. K.; Hall, J. Gordon; Golian, T. C.; and Hertzberg, A.: Boundary-Layer Displacement and Leading-Edge Bluntness Effects in High-Temperature Hypersonic Flow. J. Aerosp. Sci., vol. 28, no. 5, May 1961, pp. 353-381, 410.

5. Spalding, D. B.; and Chi, S. W.: The Drag of Compressible Turbulent Boundary Layer on a Smooth Flat Plate With and Without Heat Transfer. J. Fluid Mech., vol. 18, pt. 1, Jan. 1964, pp. 117-143.

6. Inouye, Mamoru: Shock Standoff Distance for Equilibrium Flow Around Hemispheres Obtained From Numerical Calculations. AIAA J., vol. 3, no. 1, Jan. 1965, pp. 172-173.

7. Wittliff, Charles E.; and Curtis, James T.: Normal Shock Wave Parameters in Equilibrium Air. Rep. No. CAL-111 (Contract No. AF 33(616)-6579), Cornell Aeronaut. Lab., Inc., Nov. 1961.

8. Thomas P. D.; Vinokur, M.; Bastianon, R.; and Conti, R. J.: Numerical Solution for the Three Dimensional Hypersonic Flow Field of a Blunt Delta Body. AIAA Paper No. 71-596, June 1971.

9. Wittliff, C. E.; Sundaram, T. R.; Rae, W. J.; and Lordi, J. A.: Study of High-Density Hypervelocity Flows and Similitudes. AEDC-TR-67-72, U.S. Air Force, Apr. 1967. (Available from DDC as AD 811 679.)

10. Masek, R. V.; and Forney, J. Alan: An Analysis of Predicted Space Shuttle Temperatures and Their Impact on Thermal Protection Systems. Vol. I of NASA Space Shuttle Technology Conference, NASA TM X-2272, 1971, pp. 75-96.

11. Johnson, Charles B. (With appendix B by George C. Ashby, Jr.): Boundary-Layer Transition and Heating Criteria Applicable to Space Shuttle Configurations From Flight and Ground Tests. Vol. I of NASA Space Shuttle Technology Conference, NASA TM X-2272, 1971, pp. 97-156.

12. Johnson, Charles B.; and Boney, Lillian R.: A Simple Integral Method for the Calculation of Real-Gas Turbulent Boundary Layers With Variable Edge Entropy. NASA TN D-6217, 1971.

TABLE I.- EXPERIMENTAL TEST CONDITIONS

Run	Mach number	Reynolds number, $R_{\infty,L}$	Angle of attack, deg	$T_{t,1}$, K	$p_{t,1}$, atm[a]
Delta-wing body					
3	8.04	4.66×10^6	20	808.3	102.7
4	7.99	3.37	20	780.5	69.0
5	8.04	5.05	40	780.5	105.1
6	7.99	3.37	40	780.5	69.0
10	8.04	5.04	60	769.4	102.4
11	7.99	3.41	60	775.0	69.0
12	7.91	2.06	60	725.0	36.4
Straight body					
28	8.11	8.46×10^6	0	811.1	191
29	8.03	5.19	0	730.5	96.3
30	8.03	4.53	20	783.3	96.3
31	8.11	8.97	20	783.3	191
32	8.03	4.64	40	780.5	96.3
33	8.00	9.67	40	766.7	193
34	7.95	2.32	60	777.8	47.6
35	8.04	4.89	60	769.4	95.2
36	8.00	9.75	60	761.1	192

[a] 1 atm = 1.013×10^5 N/m^2.

TABLE II.- PRESSURE DATA FOR STRAIGHT BODY

(a) Center line

$^{a}\bar{s}/R_N$	Run 28	Run 29	Run 30	Run 31	Run 32	Run 33	Run 34	Run 35	Run 36
	$p/p_{t,2}$ for angle of attack, deg, of –								
	0	0	20	20	40	40	60	60	60
1.134	0.1918	0.1948	0.5421	0.5480	0.8874	0.8439	0.9525	0.9766	0.9570
1.571	.0466	.0449	.1969	.2002	.5270	.5104	.8587	.8963	.8802
2.071	.0344	.0337	.1491	.1537	.4870	.4724	.8233	.8635	.8465
2.823	.0302	.0305	.1331	.1357	.5110	.4983	.8187	.8573	.8386
4.075	.0236	.0273	.1275	.1311	.5262	.5218	.8249	.8573	.8374
5.571	.0194	.0225	.1315	.1382	.5230	.5053	.8203	.8589	.8276
7.571	.0152	.0178	.1491	.1546	.5222	.4995	.8295	.8565	.8284
10.571	.0152	.0194	.1602	.1663	.5374	.5143	.8387	.8698	.8296
13.571	.0143	.0202	.1602	.1608	.5350	.5088	.8233	.8526	.8096
16.571	.0152	.0225	.1578	.1562	.5278	.4979	.8157	.8378	.7943
20.571	.0131	.0187	.1501	.1560	.5194	.4892	.7839	.8182	.7727
24.571	.0144	.0211	.1598	.1593	.4749	.4318	.7667	.8009	.7473
28.571	.0118	.0163	.1477	.1458	.4806	.4398	.7527	.7867	.7361
32.571	.0144	.0195	.1412	.1382	.4312	.4034	.7418	.7772	.7298

$^{a}\bar{s}$ measured from Newtonian stagnation point at $\alpha = 0^{o}$.

TABLE II.- PRESSURE DATA FOR STRAIGHT BODY – Concluded

(b) Spanwise

[a] $\bar{s}/R_N$	[b] 2z/b	Run 28	Run 29	Run 30	Run 31	Run 32	Run 33	Run 34	Run 35	Run 36
		$p/p_{t,2}$ for angle of attack, deg, of –								
		0	0	20	20	40	40	60	60	60
7.571	-0.451	0.0139	0.0178	0.1514	0.1579	0.5118	0.4908	0.8110	0.8401	0.8127
	-.180	.0139	.0194	.1491	.1529	.5214	.5018	.8249	.8542	.8269
	0	.0152	.0178	.1491	.1546	.5222	.4995	.8295	.8565	.8284
	.180	.0160	.0202	.1498	.1537	.5190	.5002	.8233	.8542	.8261
	.451	.0139	.0194	.1530	.1575	.5086	.4944	.8095	.8386	.8088
13.571	-.625	.0114	.0154	.1706	.1709	.5246	.5018	.7834	.8027	.7618
	-.438	.0118	.0170	.1658	.1663	.5334	.5135	.8064	.8355	.7931
	-.250	.0123	.0178	.1618	.1629	.5358	.5112	.8157	.8409	.8026
	-.125	.0148	.0194	.1594	.1604	.5350	.5092	.8249	.8511	.8088
	0	.0143	.0202	.1602	.1608	.5350	.5088	.8233	.8526	.8096
	.125	.0160	.0217	.1634	.1608	.5318	.5073	.8310	.8518	.8080
	.250	.0135	.0202	.1610	.1613	.5326	.5057	.8203	.8448	.8022
	.438	.0135	.0217	.1682	.1633	.5318	.5061	.8110	.8355	.7916
	.625	.0135	.0225	.1762	.1726	.5286	.5041	.7803	.8019	.7575
20.571	-.625	.0097	.0082	.1429	.1454	.4644	.4327	.7325	.7685	.7326
	-.438	.0135	.0163	.1534	.1551	.4935	.4608	.7714	.8024	.7548
	-.250	.0131	.0171	.1534	.1572	.5065	.4727	.7761	.8127	.7691
	-.125	.0127	.0154	.1517	.1577	.5194	.4826	.7870	.8190	.7723
	0	.0131	.0187	.1501	.1560	.5194	.4842	.7839	.8182	.7727
	.125	.0127	.0203	.1517	.1564	.5186	.4834	.7870	.8182	.7719
	.250	.0135	.0171	.1542	.1572	.5089	.4735	.7792	.8111	.7671
	.438	.0148	.0179	.1566	.1589	.4968	.4600	.7730	.8064	.7604
	.625	.0118	.0187	.1501	.1509	.4612	.4287	.7356	.7724	.7294
32.571	-.625	.0148	.0187	.1299	.1293	.4094	.3903	.6936	.7219	.6798
	-.438	.0157	.0187	.1372	.1348	.4272	.4053	.7232	.7519	.7095
	-.250	.0148	.0203	.1388	.1382	.4320	.4073	.7403	.7709	.7250
	-.125	.0165	.0187	.1396	.1382	.4344	.4065	.7434	.7732	.7290
	0	.0144	.0195	.1412	.1382	.4312	.4034	.7418	.7772	.7298
	.125	.0144	.0195	.1404	.1386	.4288	.4006	.7418	.7748	.7286
	.250	.0152	.0195	.1380	.1365	.4247	.4002	.7403	.7724	.7238
	.438	.0161	.0195	.1380	.1339	.4231	.3974	.7278	.7582	.7087
	.625	.0169	.0171	.1324	.1288	.4053	.3816	.6936	.7203	.6754

[a] $\bar{s}$ measured from Newtonian stagnation point at $\alpha = 0^{\circ}$.

[b] b = 5.08 cm.

TABLE III.- PRESSURE DATA FOR DELTA-WING BODY

(a) Center line

$a_{\bar{S}}/R_N$	Run 3	Run 4	Run 5	Run 6	Run 10	Run 11	Run 12
	$p/p_{t,2}$ for angle of attack, deg, of –						
	20	20	40	40	60	60	60
1.134	0.4243	0.4558	0.7932	0.7845	0.9745	0.9761	0.9540
1.571	.1710	.1882	.4849	.4720	.8886	.9367	.8570
2.071	.1355	.1459	.4620	.4438	.8651	.8494	.8314
2.823	.1243	.1347	.4944	.4691	.8593	.8466	.8314
4.075	.1184	.1347	.4963	.4832	.8475	.8466	.8264
5.571	.1262	.1431	.4868	.4889	.8475	.8382	.8161
7.571							
10.571	.1496	.1572	.4924	.4889	.8475	.8579	.8212
13.571	.1516	.1657	.4887	.4973	.8553	.8579	.8264
16.571	.1399	.1572	.4849	.4917	.8690	.8748	.8417
20.571	.1457	.1572	.5020	.5001	.8593	.8720	.8417
24.571	.1574	.1684	.4811	.4944	.8475	.8579	.8314
28.571	.1399	.1684	.5096	.5114	.8358	.8438	.8161
32.571	.1418	.1572	.4754	.4860	.8241	.8298	.8161

$a_{\bar{S}}$ measured from Newtonian stagnation point at $\alpha = 0^{\circ}$.

TABLE III.- PRESSURE DATA FOR DELTA-WING BODY – Concluded

(b) Spanwise

[a] $\bar{s}/R_N$	b, cm	2z/b	Run 3	Run 4	Run 5	Run 6	Run 10	Run 11	Run 12
			$p/p_{t,2}$ for angle of attack, deg, of –						
			20	20	40	40	60	60	60
7.571	3.277	-0.484	0.1457	0.1618	0.4849	0.4832	0.8339	0.8298	0.8110
		-.193	.1360	.1516	.4868	.4748	.8514	.8466	.8212
		0	------	------	------	------	------	------	------
		.193	.1360	.1488	.4887	.4748	.8514	.8410	.8212
		.484	.1418	.1572	.4792	.4748	.8299	.8241	.8008
13.571	5.258	-.664	------	------	------	------	------	------	------
		-.483	.1554	.1684	.4868	.4944	.8397	.8438	.8161
		-.302	.1477	.1628	.4887	.4944	.8494	.8494	.8212
		-.121	.1516	.1657	.4887	.4973	.8534	.8607	.8264
		0	.1516	.1657	.4887	.4973	.8553	.8579	.8264
		.121	.1558	.1657	.4906	.4973	.8553	.8607	.8264
		.302	.1516	.1657	.4906	.4973	.8494	.8523	.8264
		.483	.1554	.1657	.4906	.4917	.8378	.8410	.8110
		.664	.1593	.1684	.4811	.4860	.8124	.8184	.7854
20.571	7.569	-.798	.1574	.1741	.4697	.4804	.7928	.7847	.7651
		-.588	.1516	.1684	.4868	.4860	.8553	.8579	.8212
		-.378	.1477	.1628	.4982	.4944	.8612	.8720	.8366
		-.210	.1477	.1600	.5001	.4973	.8593	.8720	.8366
		-.084	.1457	.1572	.5020	.5001	.8593	.8720	.8366
		0	.1457	.1572	.5020	.5001	.8593	.8720	.8417
		.084	.1457	.1572	.5020	.5001	.8593	.8748	.8417
		.210	.1477	.1600	.4982	.5001	.8612	.8748	.8468
		.378	.1477	.1684	.4924	.4973	.8632	.8748	.8468
		.588	.1535	.1741	.4849	.4973	.8534	.8466	.8314
		.798	.1574	.1769	.4678	.4832	.7811	.7819	.7549
32.571	11.506	-.856	.1328	.1741	.4639	.4776	.7440	.7481	.7344
		-.635	.1516	.1657	.4792	.4944	.8045	.8101	.7906
		-.414	.1457	.1628	.4899	.5086	.8202	.8241	.8110
		-.249	.1457	.1628	.4811	.5029	.8221	.8269	.8161
		-.138	.1457	.1628	.4811	.4944	.8241	.8298	.8161
		-.055	.1418	.1572	.4754	.4860	.8241	.8258	.8161
		0	.1418	.1572	.4754	.4860	.8241	.8298	.8161
		.055	.1438	.1572	.4734	.4889	.8241	.8298	.8161
		.138	.1399	.1572	.4716	.4917	.8221	.8269	.8110
		.249	.1438	.1600	.4754	.5001	.8221	.8269	.8110
		.414	.1438	.1600	.4754	.5001	.8182	.8241	.8059
		.635	.1477	.1600	.4716	.4832	.8026	.8101	.7957
		.856	.1554	.1713	.4527	.4720	.7381	.7424	.7344

[a] $\bar{s}$ measured from Newtonian stagnation point at $\alpha = 0^{\circ}$.

TABLE IV.- NONEQUILIBRIUM EFFECTS ON SURFACE STREAMLINE TEMPERATURE

Trajectory point				T_{eq}, K	T_{neq}, K (a)
V		h			
km/sec	ft/sec	km	ft		
4.877	16 000	60.96	200 000	4178	3459
6.096	20 000	67.06	220 000	4973	3721
7.315	24 000	76.20	250 000	5198	3372

[a] At S_b = 45.7 meters (150 ft).

TABLE V.- NONEQUILIBRIUM EFFECTS ON OUTER STREAMLINE TEMPERATURE

$[\alpha = 20^{o};\ R_N = 1.22\ m\ (4\ ft)]$

Trajectory point				T_{eq}, K	T_{neq}, K (a)
V		h			
km/sec	ft/sec	km	ft		
4.877	16 000	60.96	200 000	2053	2120
6.096	20 000	67.06	220 000	2486	2997
7.315	24 000	76.20	250 000	2707	3720

[a] At S_b = 45.7 meters (150 ft).

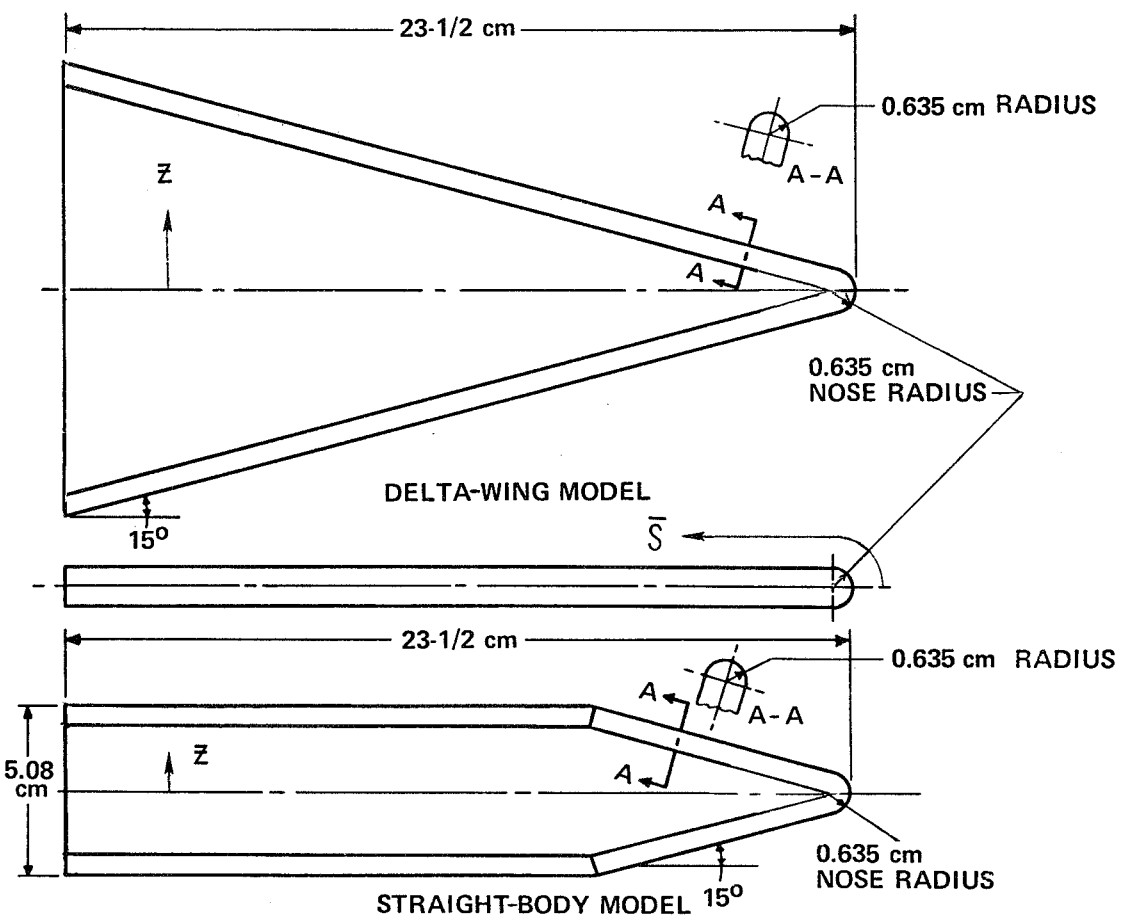

Figure 1.- Delta-wing and straight-body models for wind-tunnel pressure measurements.

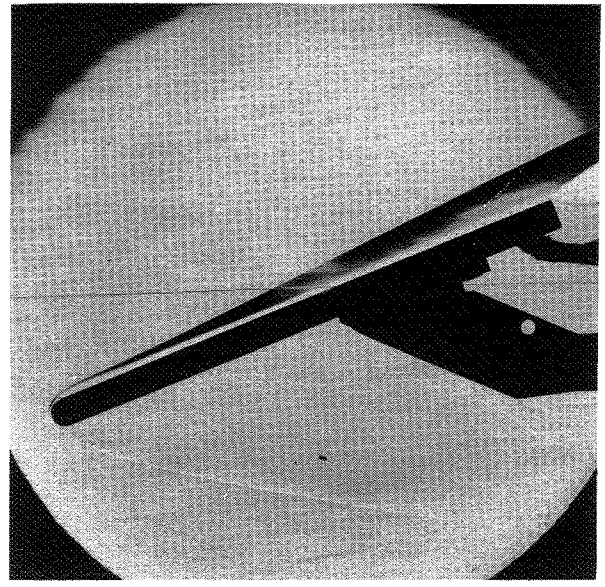

DELTA-WING BODY
$R_{\infty,L} = 4.66 \times 10^6$

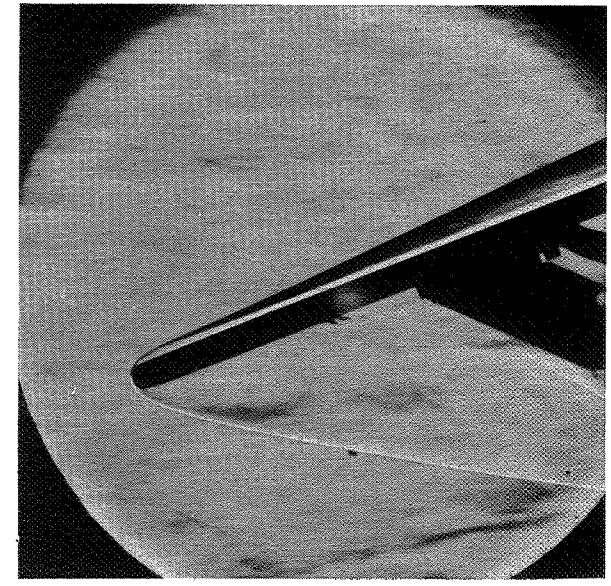

STRAIGHT BODY
$R_{\infty,L} = 8.97 \times 10^6$

L-73-282

(a) $\alpha = 20^{\circ}$.

Figure 2.- Schlieren photographs of model flow fields.

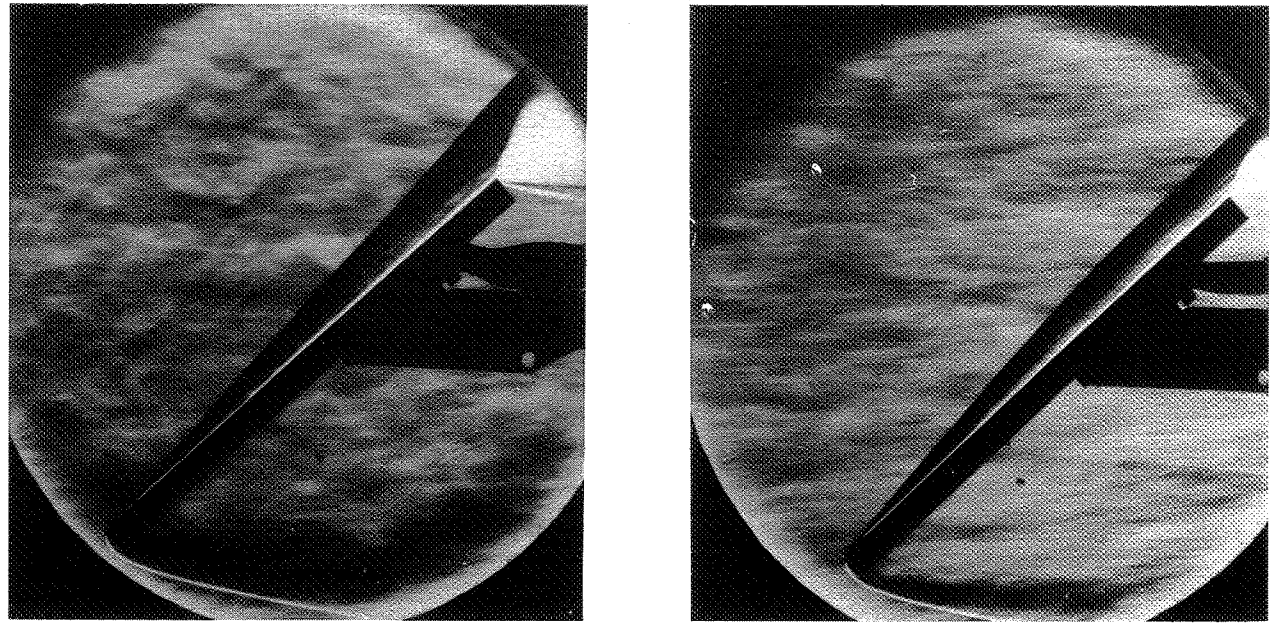

DELTA-WING BODY
$R_{\infty,L} = 5.05 \times 10^6$

STRAIGHT BODY
$R_{\infty,L} = 9.67 \times 10^6$

L-73-283

(b) $\alpha = 40^{\circ}$.

Figure 2.- Continued.

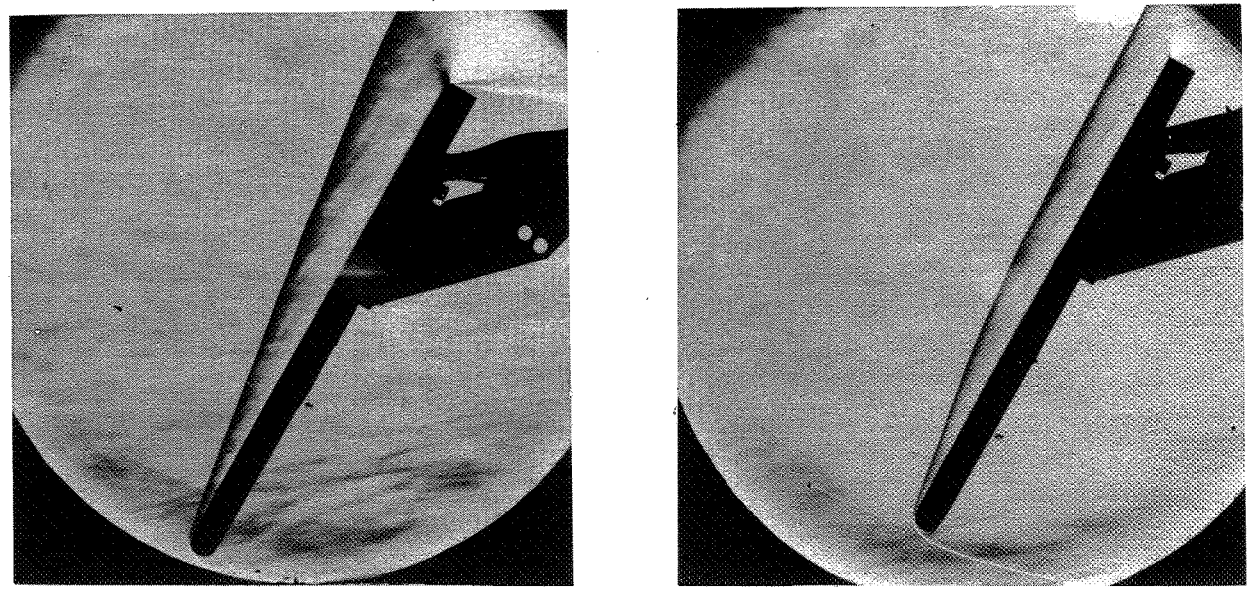

DELTA-WING BODY
$R_{\infty,L} = 5.04 \times 10^6$

STRAIGHT BODY
$R_{\infty,L} = 2.32 \times 10^6$

L-73-284

(c) $\alpha = 60^{\circ}$.

Figure 2.- Concluded.

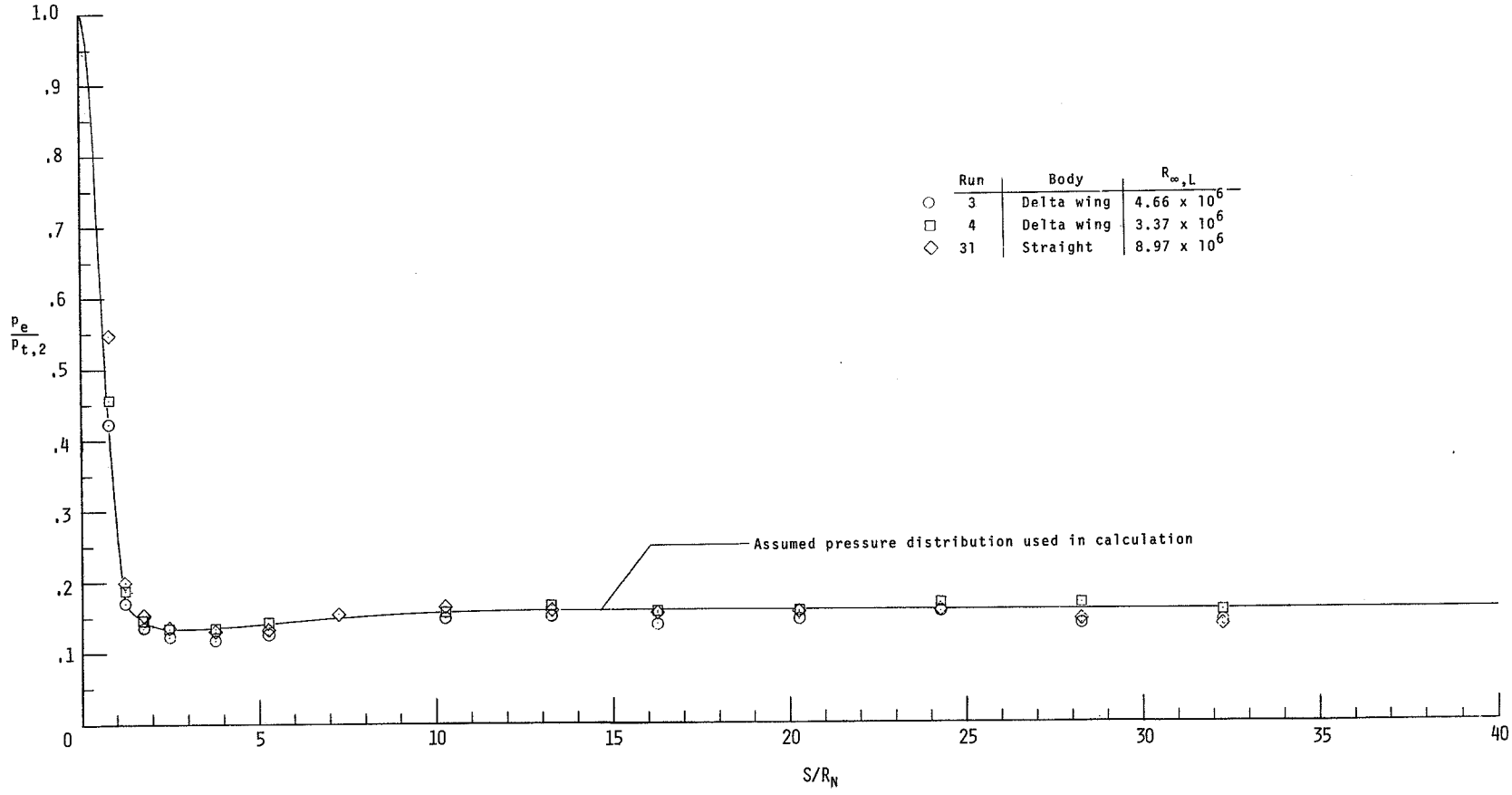

(a) $\alpha = 20^o$.

Figure 3.- Pressure distribution along windward center line.

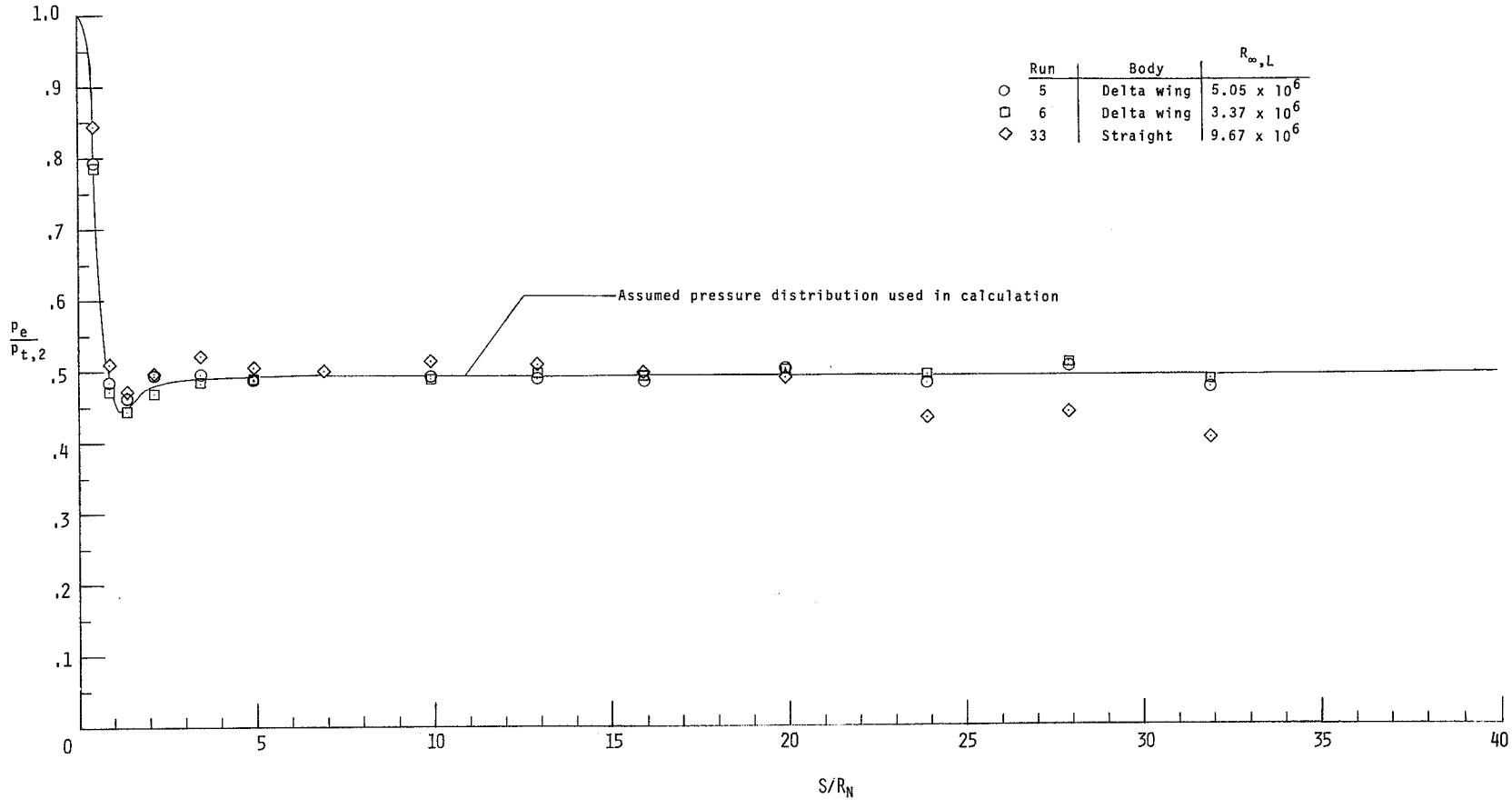

(b) $\alpha = 40^{o}$.

Figure 3.- Continued.

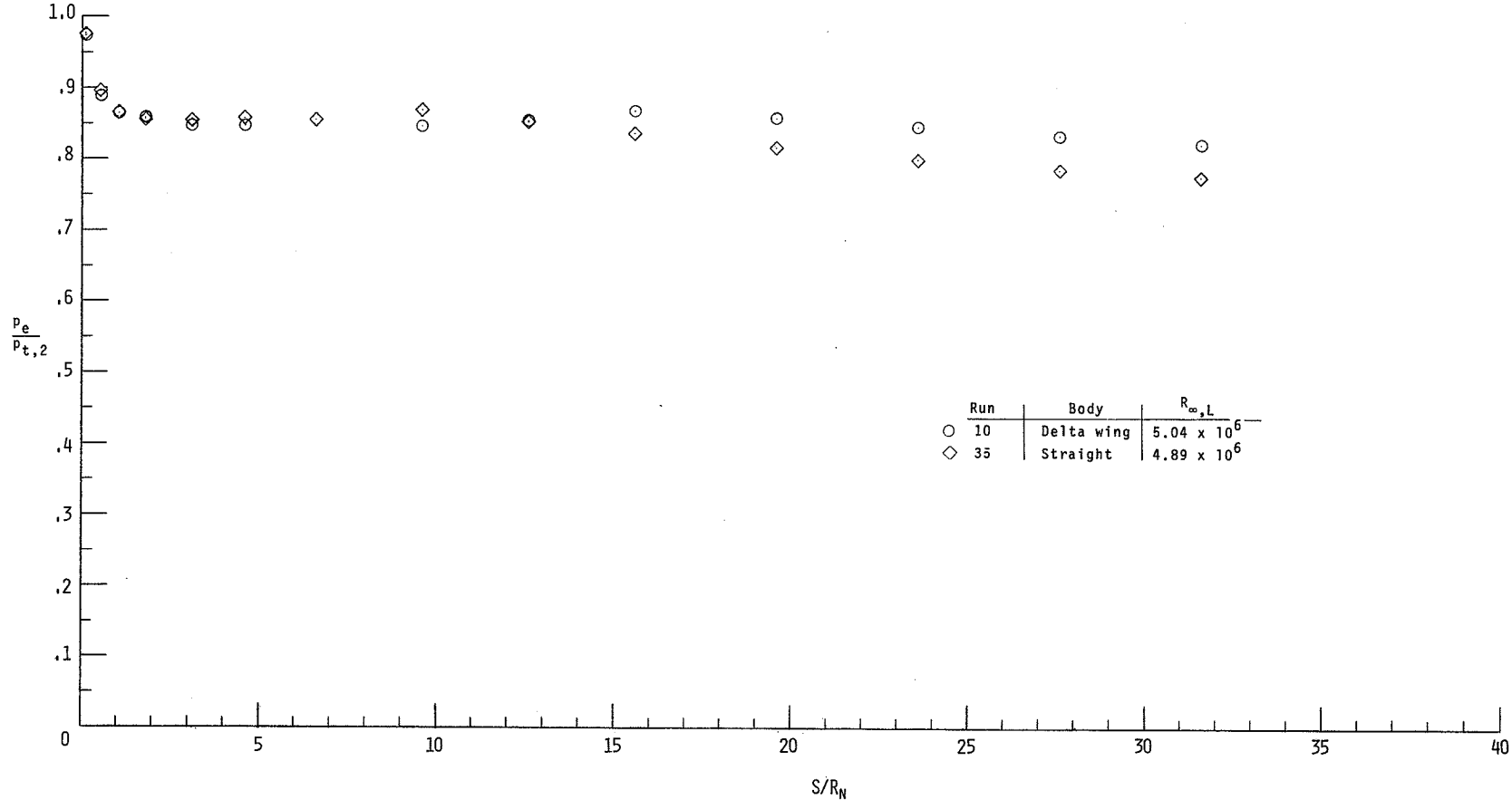

(c) $\alpha = 60^o$.

Figure 3.- Concluded.

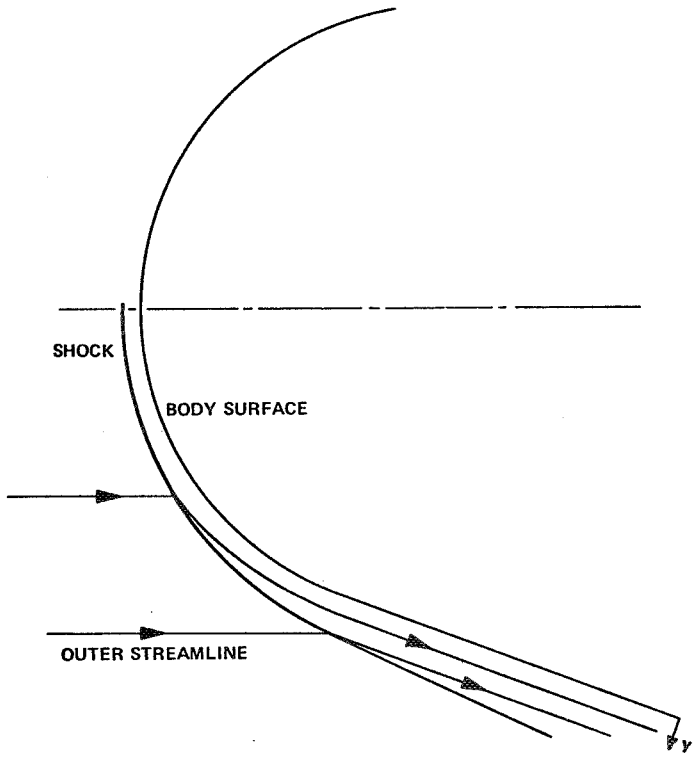

$\alpha = 20^{o}$

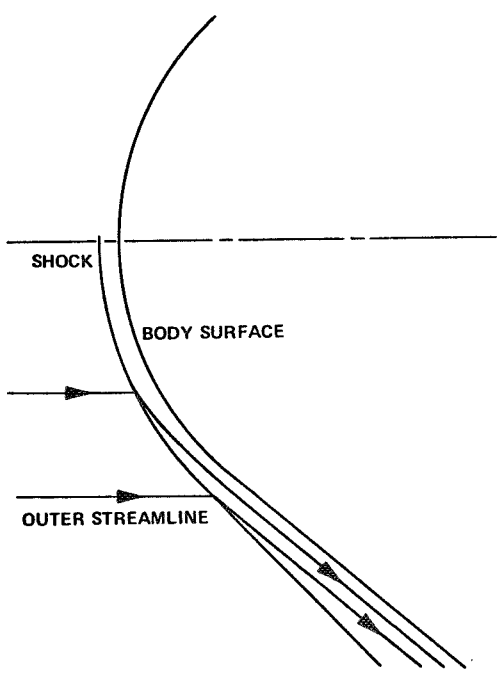

$\alpha = 40^{o}$

Figure 4.- Shock shape and streamline pattern in nose region.

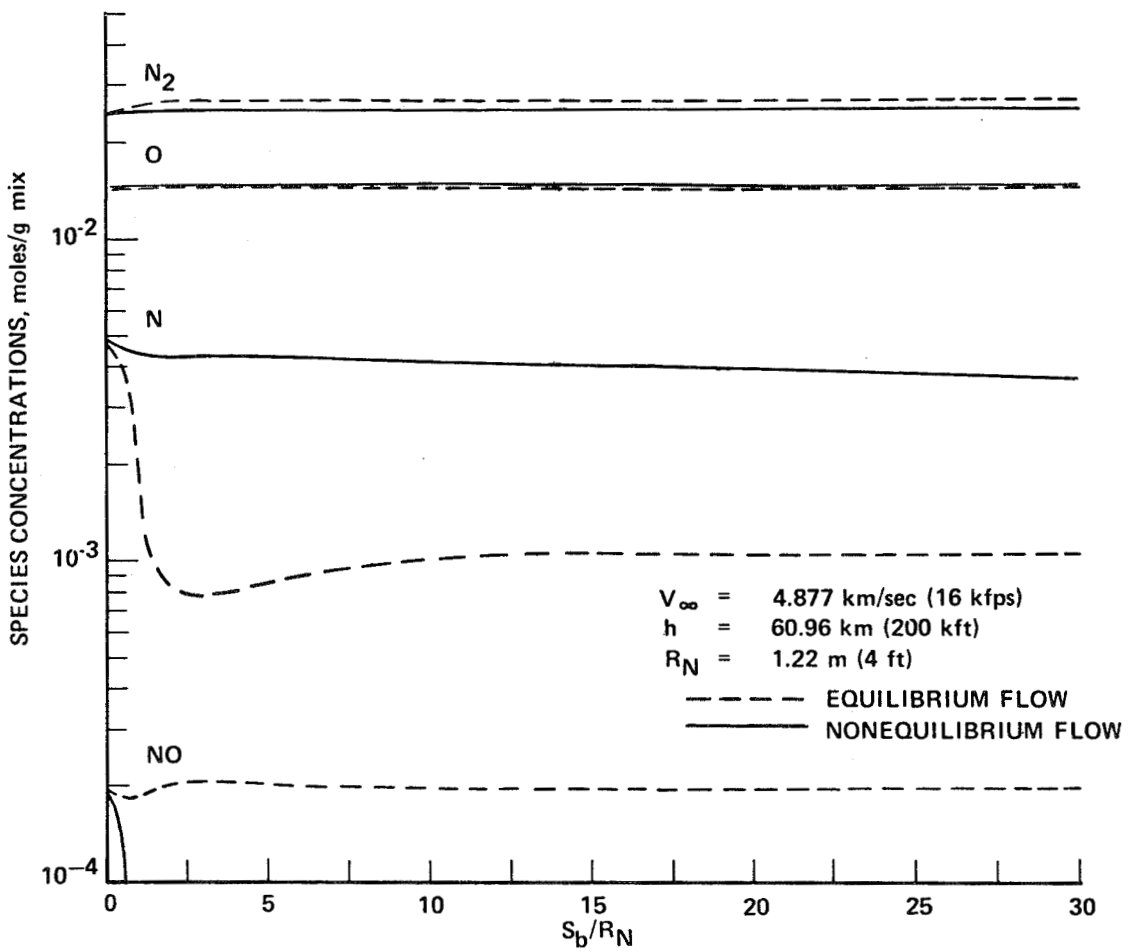

Figure 5.- Nonequilibrium effect on species concentrations along body surface streamline.

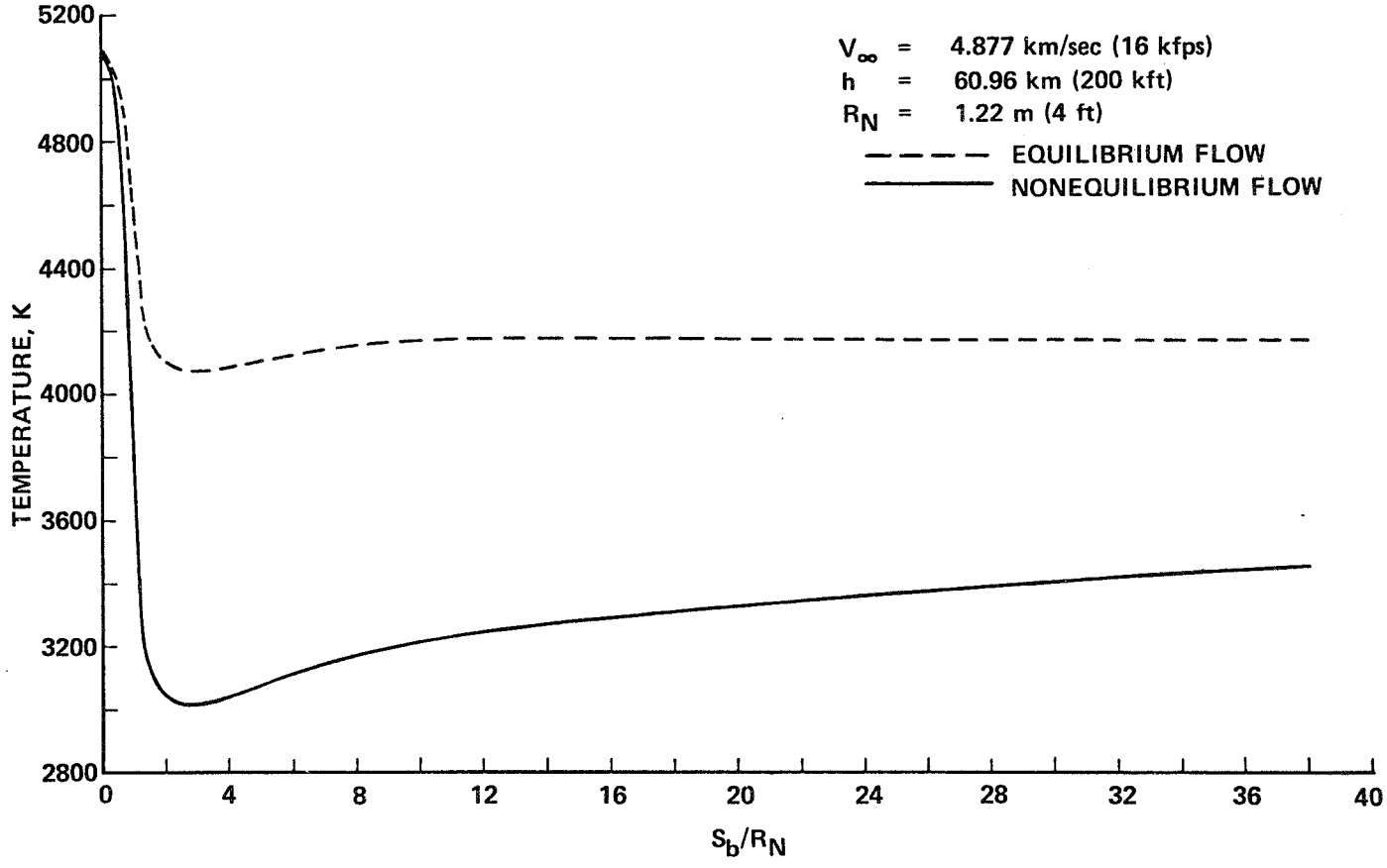

(a) Effect on temperature.

Figure 6.- Nonequilibrium effect along body surface streamline. $\alpha = 20^{o}$.

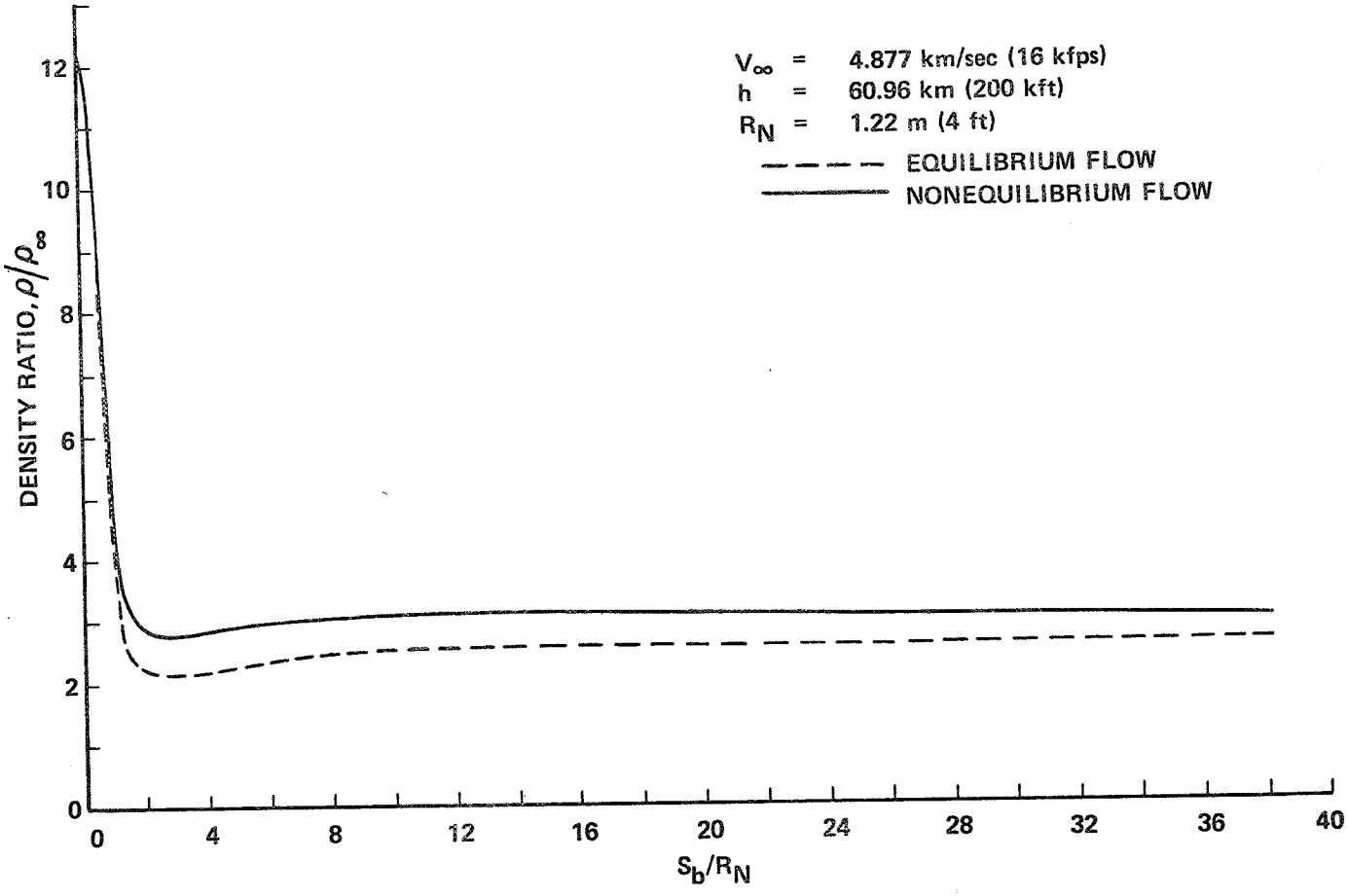

(b) Effect on density.

Figure 6.- Continued.

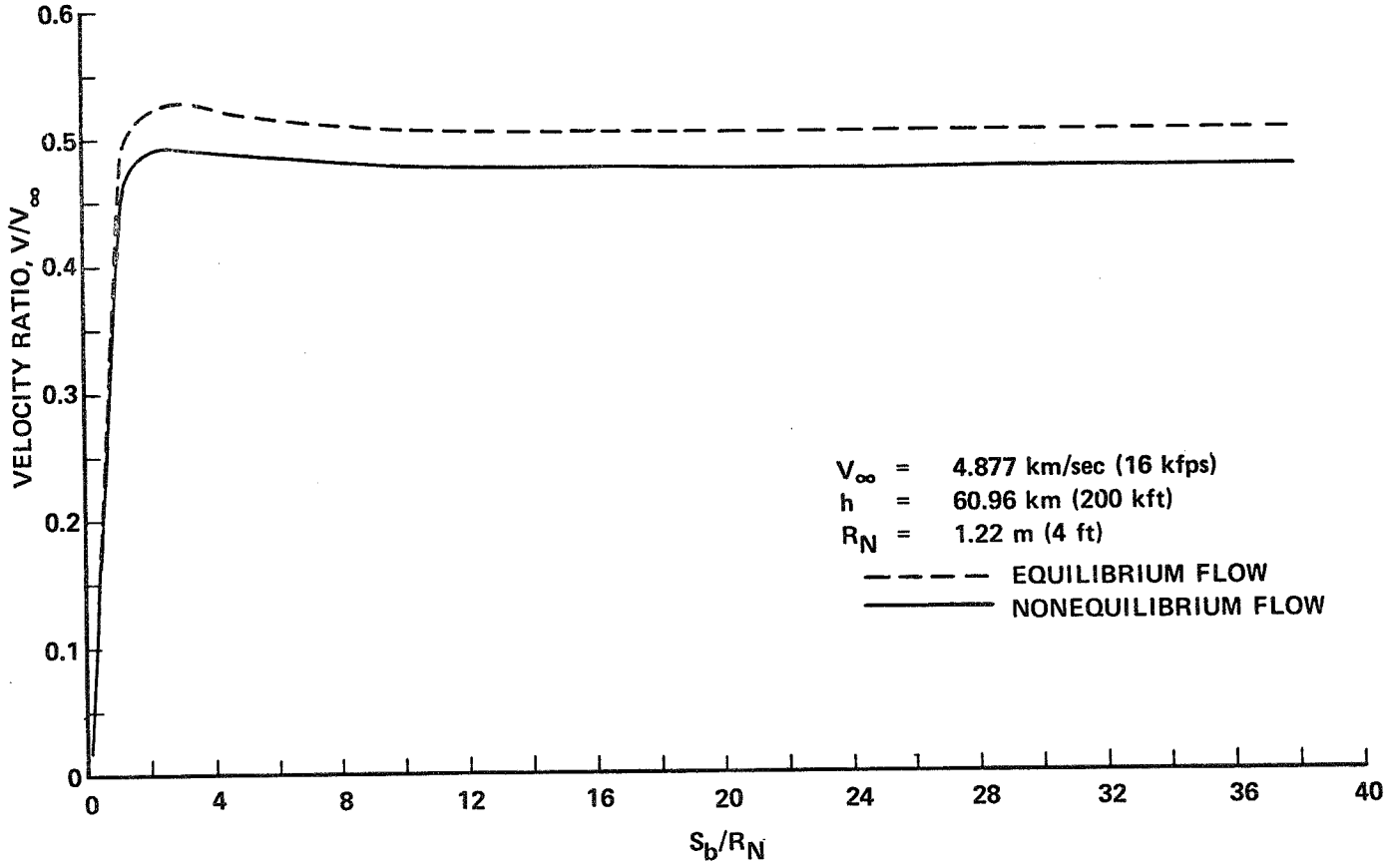

(c) Effect on velocity.

Figure 6.- Concluded.

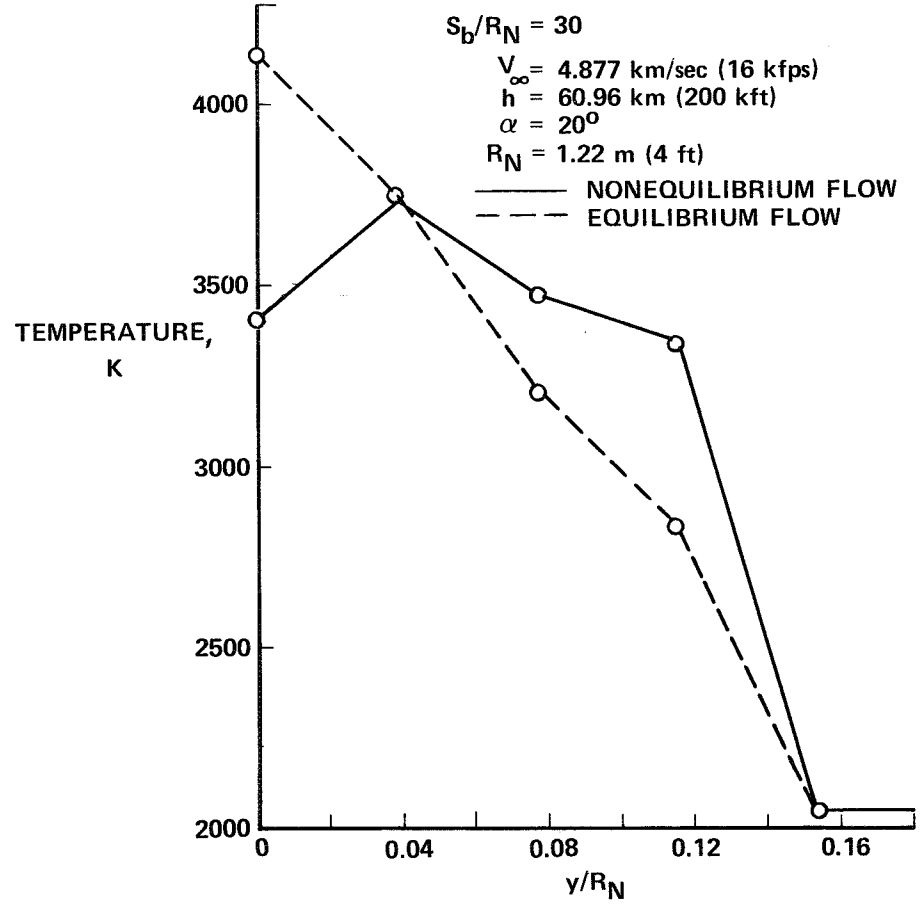

Figure 7.- Nonequilibrium effect on temperature distribution through shock layer.

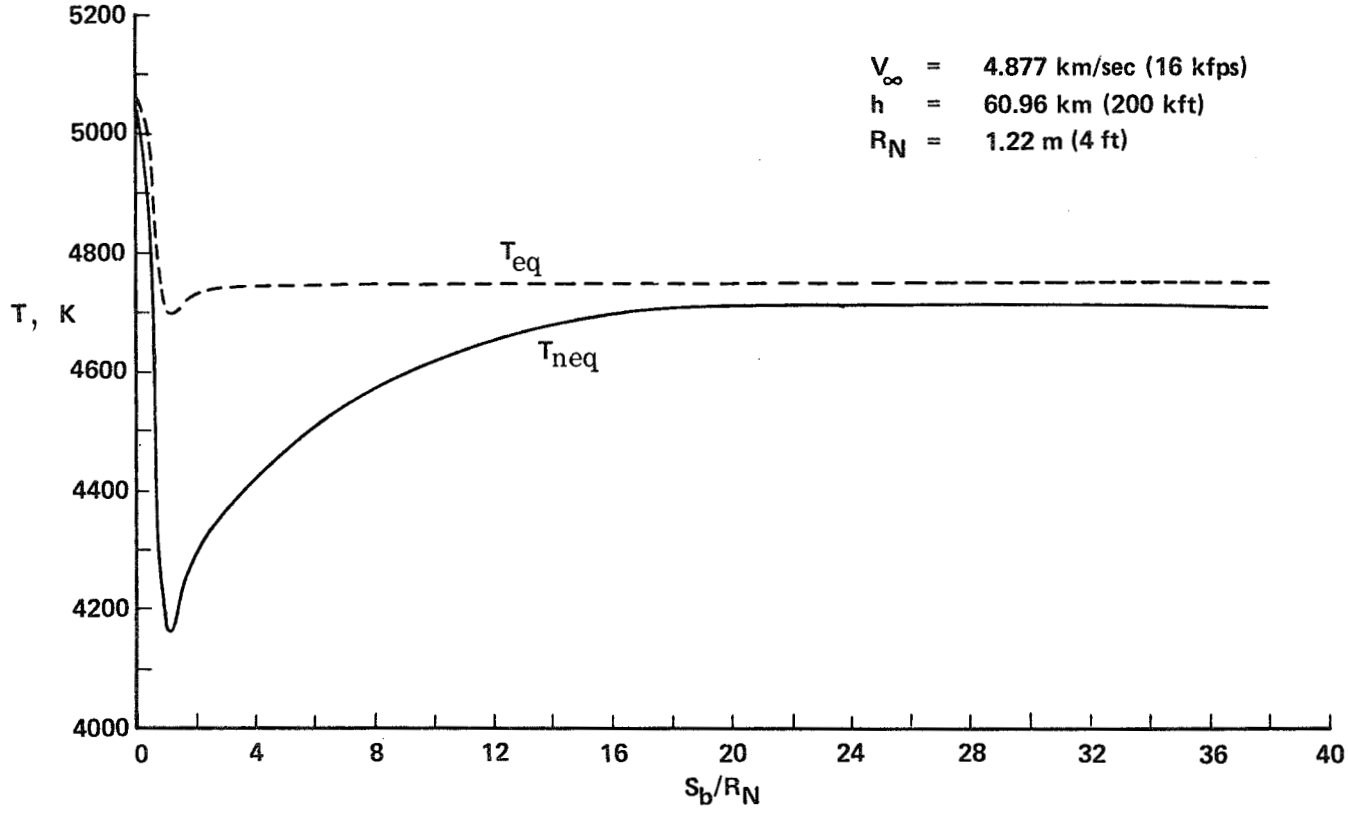

Figure 8.- Nonequilibrium effect on temperature along body surface streamline. $\alpha = 40^o$.

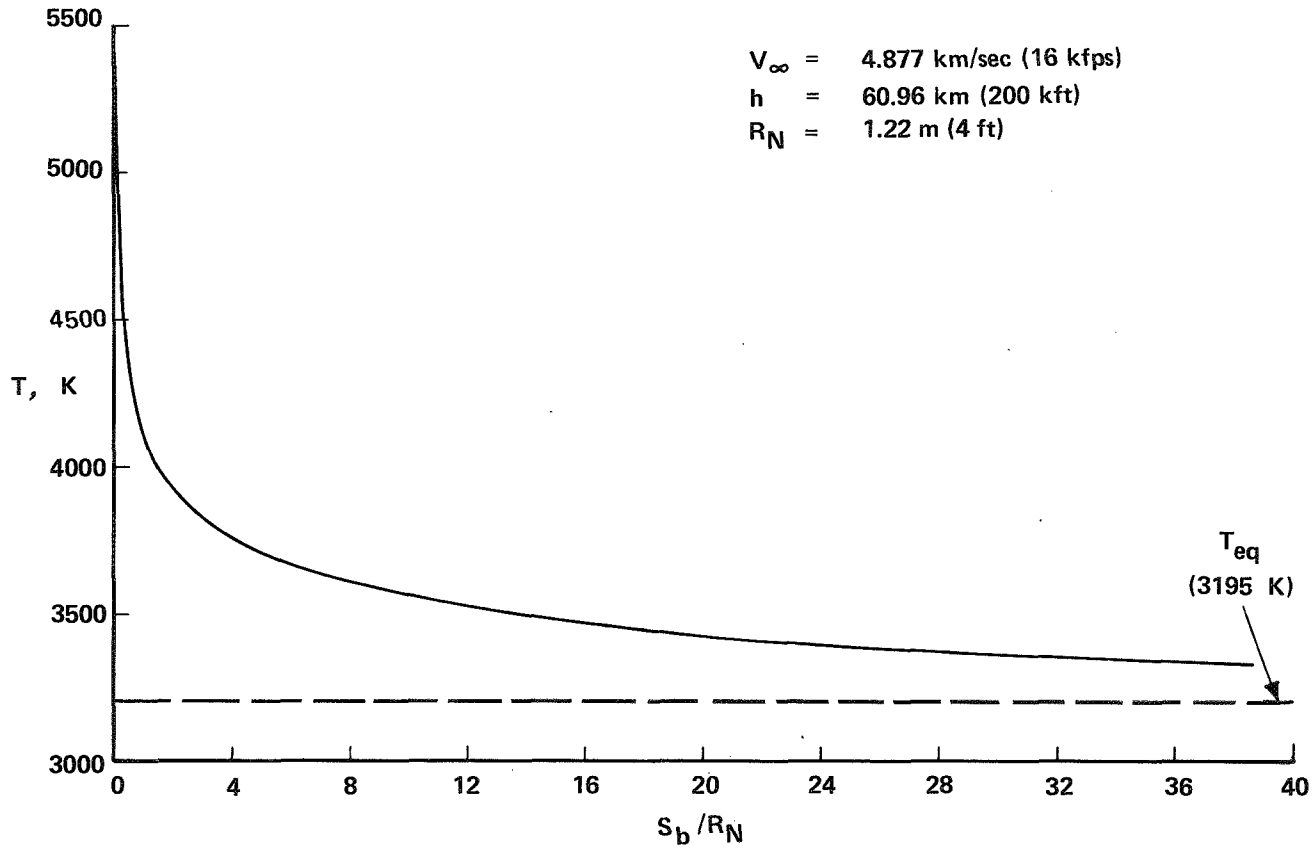

Figure 9.- Nonequilibrium effect on temperature along outer streamline. $\alpha = 40^o$.

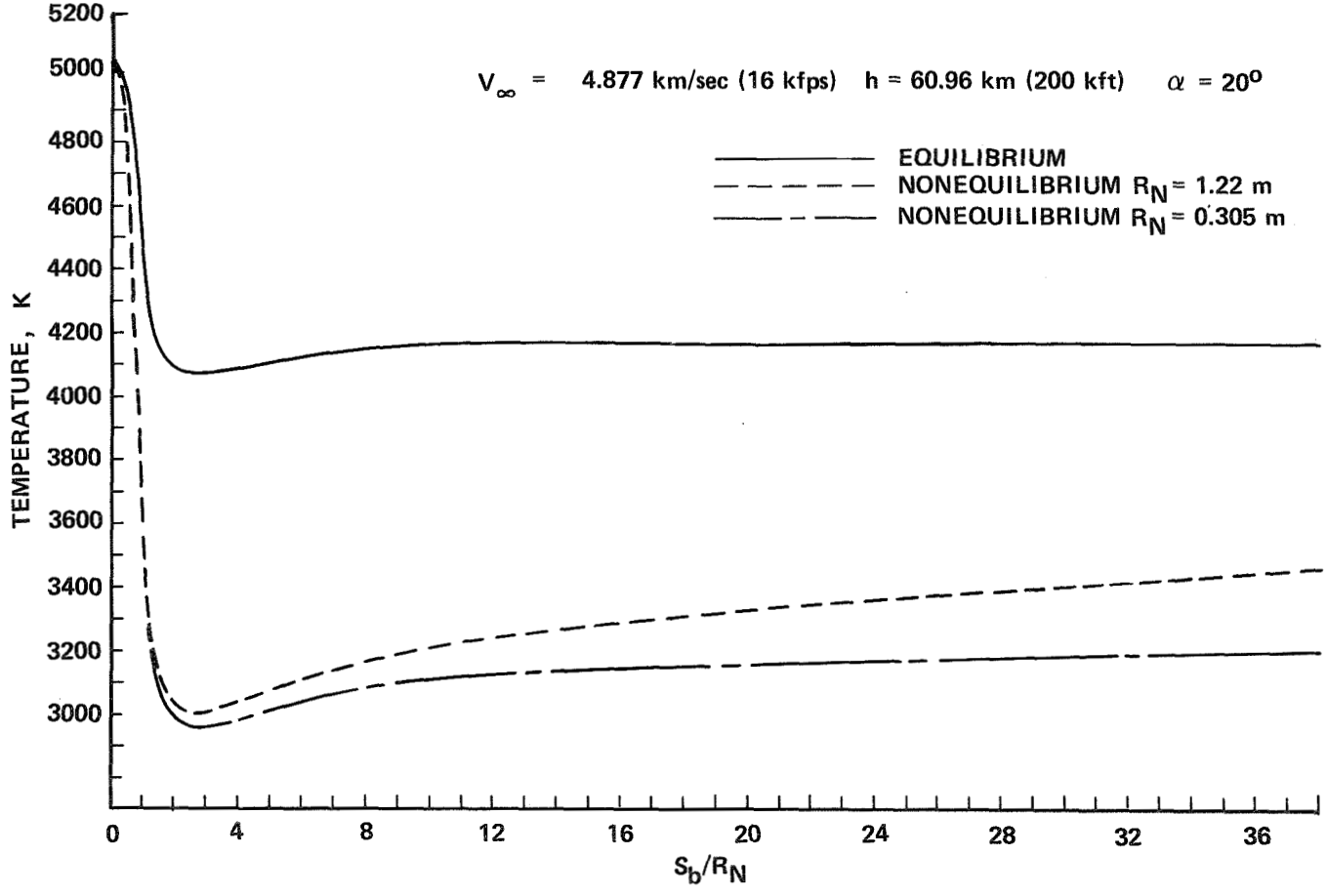

Figure 10.- Effect of nose bluntness on body surface streamline temperature distribution.

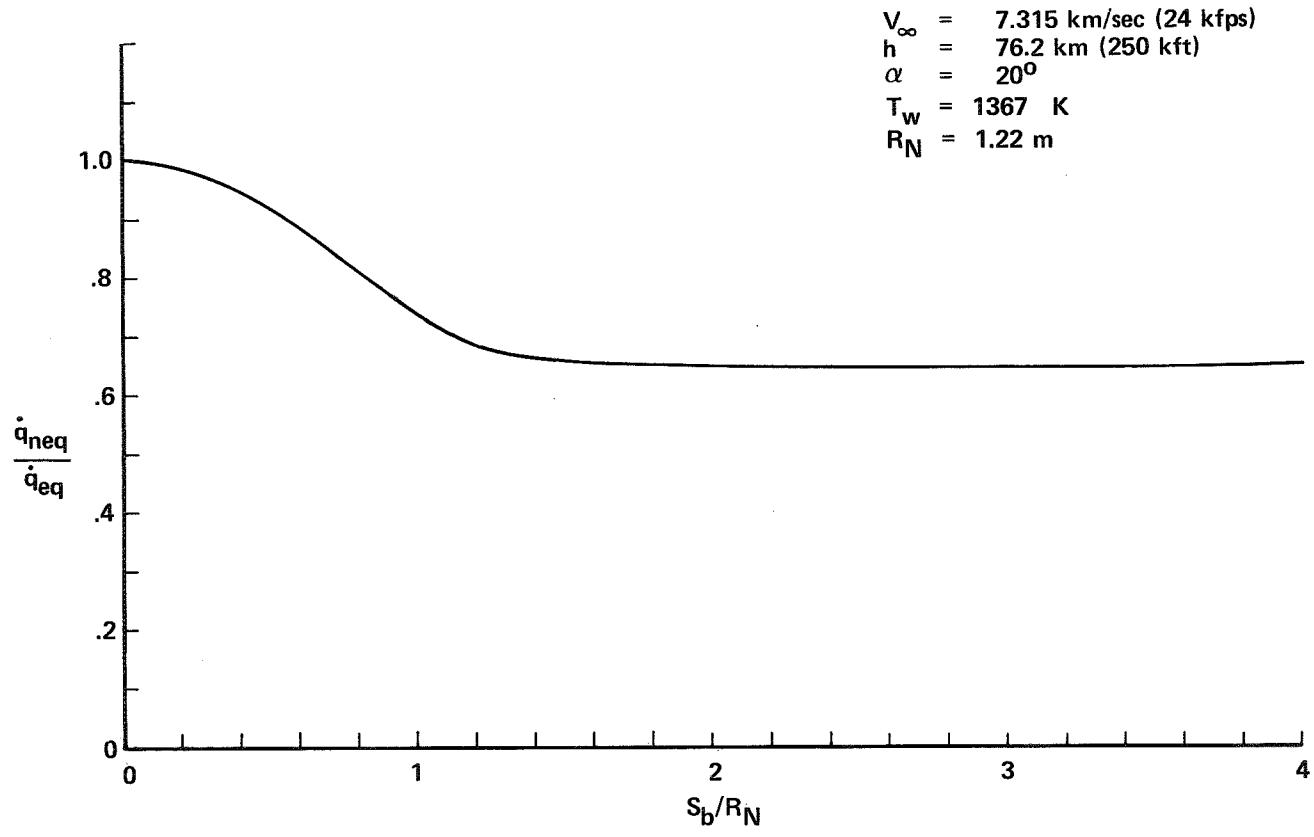

Figure 11.- Influence of nonequilibrium inviscid flows on laminar heating rate of frozen boundary layer on a noncatalytic surface.

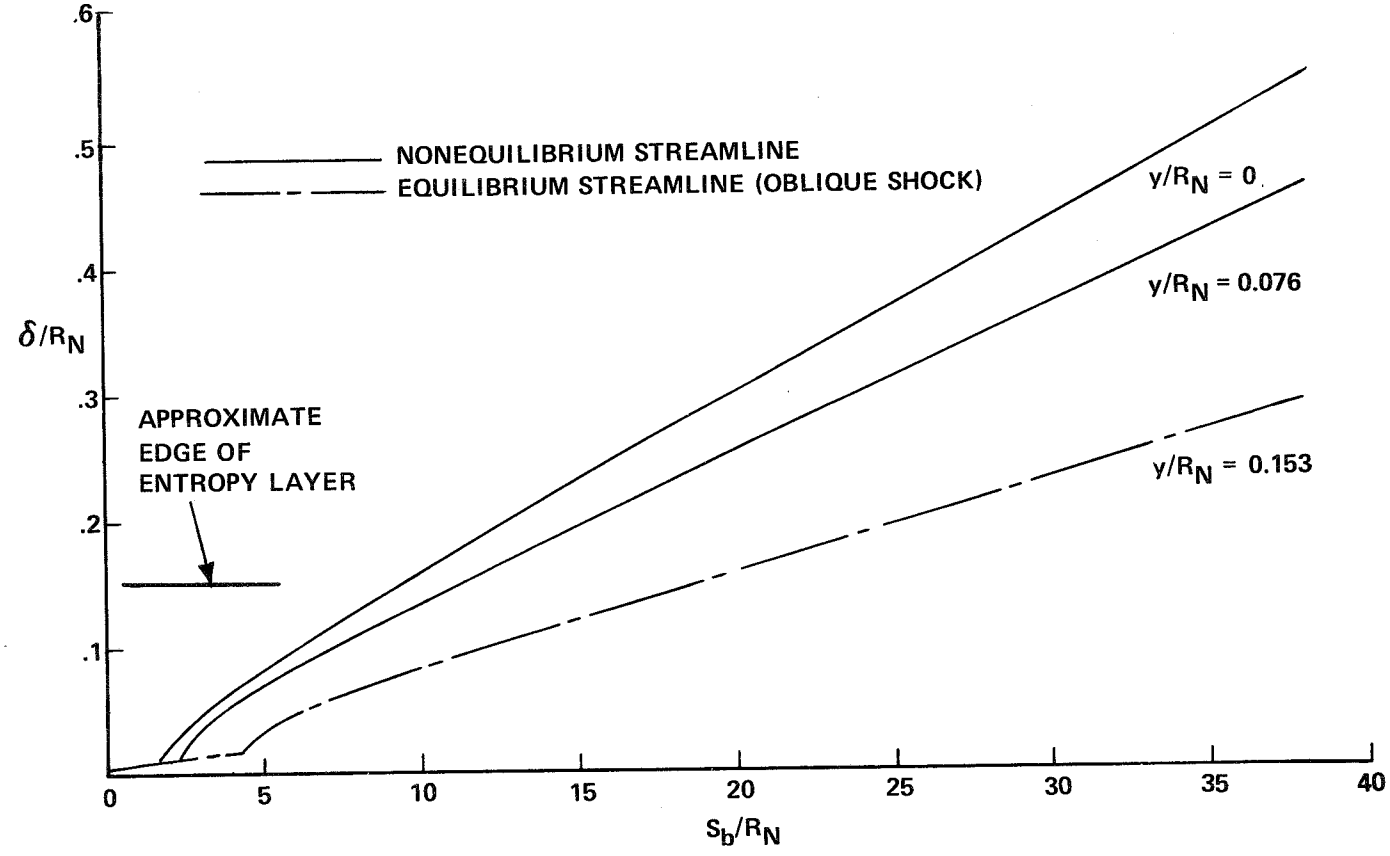

(a) V_∞ = 4.877 km/sec (16 000 ft/sec); h = 60.96 km (200 000 ft).

Figure 12.- Estimated boundary-layer thickness. $\alpha = 20^o$; R_N = 1.22 m (4 ft).

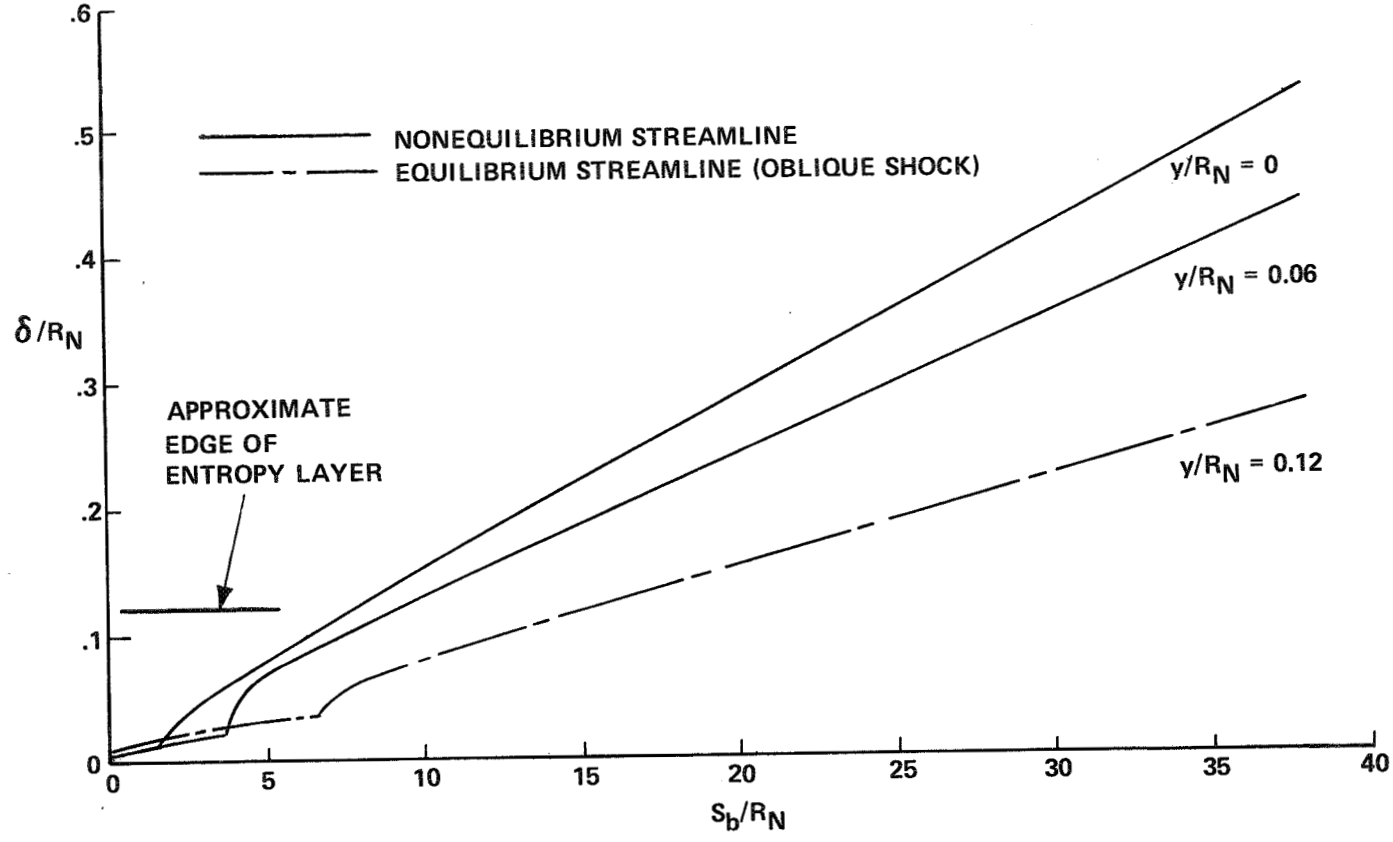

(b) V_∞ = 6.096 km/sec (20 000 ft/sec); h = 67.06 km (220 000 ft).

Figure 12.- Continued.

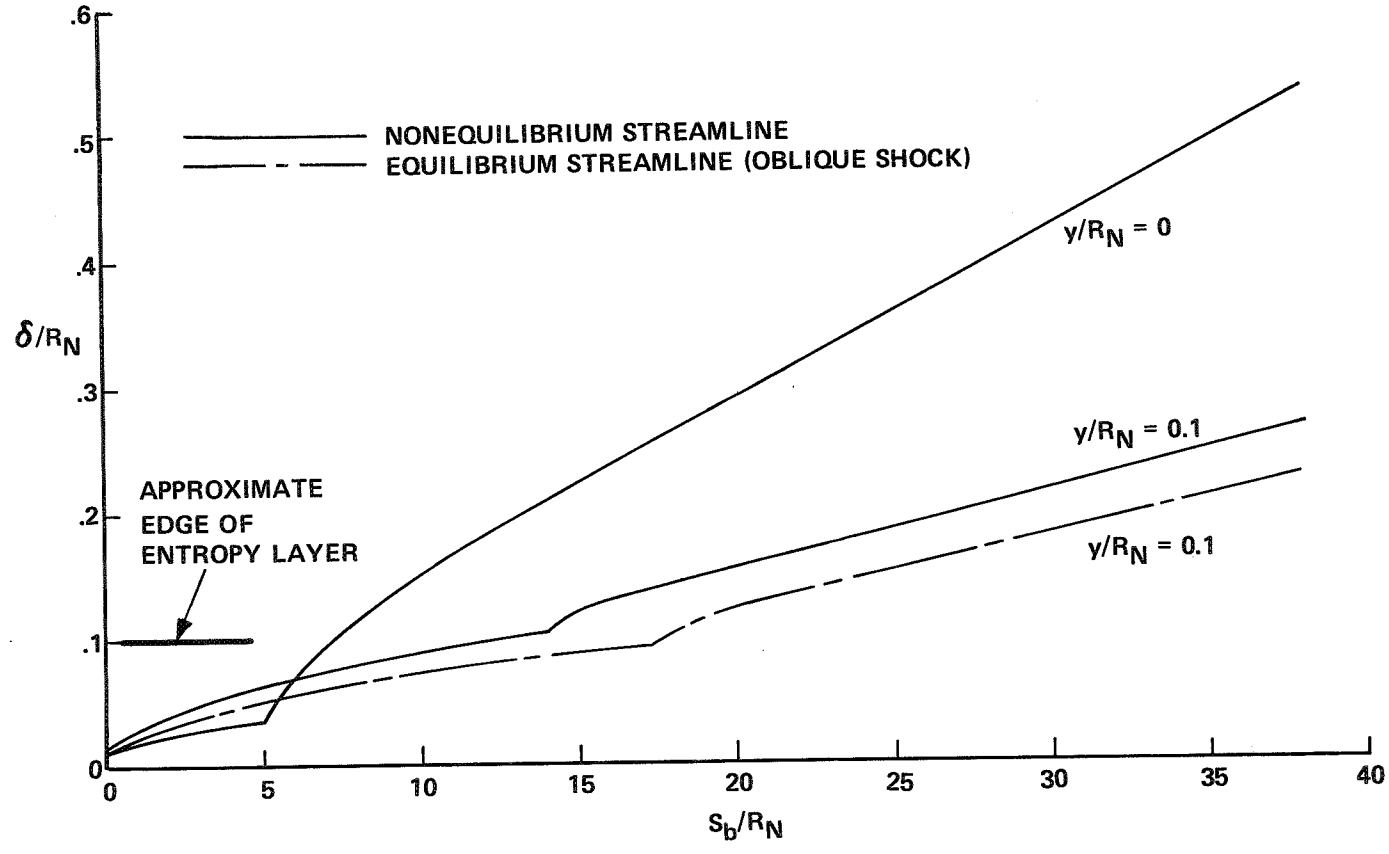

(c) V_∞ = 7.315 km/sec (24 000 ft/sec); h = 76.20 km (250 000 ft).

Figure 12.- Concluded.